



UNIVERSIDAD DE INVESTIGACION DE TECNOLOGIA EXPERIMENTAL YACHAY

Escuela de Ciencias Físicas y Nanotecnología

**TÍTULO: First Principles and Machine Learning
Investigations into the Atomic and Mechanical
Properties of Cement Hydrates (C-S-H).**

Trabajo de integración curricular presentado como requisito para
la obtención del título de Físico

Autor:

Balarezo J. Gabriel

Tutor:

Ph.D - Pinto Henry

Urcuquí, Junio 2025

AUTORÍA

Yo, **Balarezo Balarezo Juan Gabriel**, con cédula de identidad 0106019219, declaro que las ideas, juicios, valoraciones, interpretaciones, consultas bibliográficas, definiciones y conceptualizaciones expuestas en el presente trabajo; así como, los procedimientos y herramientas utilizadas en la investigación, son de absoluta responsabilidad de el/la autora (a) del trabajo de integración curricular. Así mismo, me acojo a los reglamentos internos de la Universidad de Investigación de Tecnología Experimental Yachay.

Urcuquí, junio 2025.

Juan Gabriel Balarezo Balarezo

C.I: 0106019219

AUTORIZACIÓN DE PUBLICACIÓN

Yo, **Balarezo Balarezo Juan Gabriel**, con cédula de identidad 0106019219, cedo a la Universidad de Investigación de Tecnología Experimental Yachay, los derechos de publicación de la presente obra, sin que deba haber un reconocimiento económico por este concepto. Declaro además que el texto del presente trabajo de titulación no podrá ser cedido a ninguna empresa editorial para su publicación u otros fines, sin contar previamente con la autorización escrita de la Universidad.

Asimismo, autorizo a la Universidad que realice la digitalización y publicación de este trabajo de integración curricular en el repositorio virtual, de conformidad a lo dispuesto en el Art. 144 de la Ley Orgánica de Educación Superior

Urcuquí, junio 2025.

Juan Gabriel Balarezo Balarezo

C.I: 0106019219

Contents

Contents	iii
List of Figures	v
List of Tables	vi
1 Introduction	1
1.1 Background	1
1.2 Problem Statement	2
1.3 General and Specific Objectives	2
1.4 Overview	2
2 Theoretical Background	4
2.1 Many Body Schrödinger Equation	4
2.1.1 The Coulomb Interaction	4
2.1.2 The Time-Independent Schrödinger Equation	5
2.2 The Born-Oppenheimer Approximation	7
2.3 Hartree-Fock Approximation	8
2.3.1 The Pauli Exclusion Principle	10
2.3.2 The Hartree-Fock Equations	10
2.4 Density Functional Theory	11
2.4.1 First Hohenberg-Kohn Theorem	12
2.4.2 Second Hohenberg-Kohn Theorem	13
2.4.3 Kohn-Sham Equations	14
2.4.4 Exchange-Correlation Functionals	15
2.4.4.1 Local Density Approximation	15
2.4.4.2 Generalised Gradient Approximation	16
2.4.4.3 Hybrid Functionals	17
2.5 Ab initio Molecular Dynamics	19
2.5.1 Hellmann-Feynman Theorem	19
2.5.2 Born-Oppenheimer Molecular Dynamics	20
2.6 Computational Implementation in VASP	21
2.6.1 Pseudopotentials	22
2.6.2 Projector Augmented-Wave (PAW) Method in VASP	23
2.6.2.1 Key Concepts	23
2.6.2.2 Projector Augmented-Wave (PAW) Method	26
2.6.3 Equation of State (EOS)	27
2.6.4 Machine Learning Force Fields (MLFFs)	27

2.7 Density Functional Tight Binding (DFTB+)	29
3 Methodology	30
3.1 Initial CSH Structure	30
3.2 VASP Workflow	30
3.3 VASP Input & Output Files	30
3.3.1 Input Files	31
3.3.2 Output Files	31
3.4 Strucure Optimisation and Relaxation	31
3.4.1 Initial Relaxation with DFTB+	31
3.4.2 Full Structure Relaxation with VASP	31
3.5 Machine Learning Force Field Generation	31
3.5.1 MLFF Training	31
3.5.2 MLFF Refinement	31
3.5.3 MLFF Testing	31
4 Results & Discussion	34
4.1 Convergency Tests	34
4.1.1 Cut-off Energy	34
4.1.2 K-Points Sampling	34
4.2 Density of States (DOS)	34
Bibliography	36

List of Figures

1.1	A four-level model representing the upscaling of C-S-H properties from the nanoscale to the engineering scale. (a) snapshot of C-S-H's nanostructure. (b) microstructure of C-S-H created by agglomeration of randomly oriented C-S-H nanoparticles. (c) microtexture of hardened paste composed by hydration products. (d) macrotexture of cement paste at the engineering scale. Adapted from ⁹ .	2
2.1	Jacob's ladder of exchange-correlation functionals as proposed by J. Perdew ²⁸ . The ladder categorises the functionals into rungs, from the simplest approximation (LDA) at the bottom, progressing to more sophisticated and accurate approximations (Generalised Random Phase) at the uppermost rung.	18
2.2	On-the-fly force field generation pipeline in VASP ⁴² . First, the algorithm reads the existing MLFF if available; otherwise it generates a new one. If accurate enough, a new structure is generated using the force field; otherwise, a first principles calculation is performed. If the predicted uncertainty is too large, the new structure is added to the dataset, and the force field is retrained. This oscillating process between training and prediction continues until we reach the total number of ionic steps specified in the setup.	28
3.1	Molecular model of C-S-H proposed by Ref. ⁴⁴ . Lavender and white spheres are oxygen and hydrogen from water molecules respectively; light blue and brown spheres are inter and intra-layer calcium ions, respectively; electric blue and red spheres are silicon and oxygen atoms from silica tetrahedra, respectively.	31
3.2	Self-consistent field (SFC) cycle in VASP for DFT calculations adapted from Ref. ¹¹ . The entire cycle starts with an initial guess of the electronic density $n_0(\mathbf{r})$, which then is used to calculate the effective potential $v_{\text{eff}}(\mathbf{r})$. Then, the resulting potential is used to solve the Kohn-Sham equations, from which single-electron wavefunctions $\psi_i(\mathbf{r})$ are obtained. Consequently, the new electronic density $n_{i+1}(\mathbf{r})$ is calculated. Should the old and new densities be close enough—up to a predefined threshold—the cycle stops, and the final electronic density is used to calculate the energies, forces and stress tensor of the system. Otherwise, the cycle repeats itself until convergence is achieved.	32
3.3	Unit cell structure in fractional coordinates for the C–S–H (Calcium-Silicate-Hydrate) system. The lattice vectors, atomic species (99 Ca, 60 Si, 323 O, 208 H), and the first 9 atomic positions are shown. All coordinates are expressed in direct (fractional) form.	33
4.1	A schematic representation of the DFT formalism. The many-body wavefunction is replaced by a single-particle wavefunction, which is used to calculate the electron density. The electron density is then used to calculate the total energy of the system. Adapted from ¹⁰ .	35

List of Tables

Chapter 1

Introduction

1.1 Background

Concrete is the synthetic material currently produced in volumes larger than any other material on Earth. With an annual consumption of approximately 35 billion tonnes, it is only second to water in terms of global usage^{1,2}. As the backbone of modern infrastructure, it provides the foundations for buildings, bridges, roads, dams, and other structures essential for societal development. Its widespread adoption arises from a unique combination of strength, versatility, and cost-effectiveness³, rendering it indispensable to the construction industry.

Nevertheless, despite the ubiquity of concrete, the properties of its key constituent, cement, remain incompletely understood. Cement is a chemically complex material, composed of a heterogeneous mixture of minerals that undergo a series of hydration reactions upon contact with water. The principal product of cement hydration—and the primary binding phase of concrete—calcium silicate hydrate (C-S-H)¹ is the responsible for the mechanical strength, chemical and transport properties and durability of hardened cement paste and, consequently, of concrete itself^{4,5,6,7}. Therefore, understanding the atomic and mechanical properties of C-S-H is of the uttermost importance to better formulate cementitious materials with enhanced performance and durability.⁸

In the last two decades, significant efforts have been made to

¹Cement chemistry nomenclature

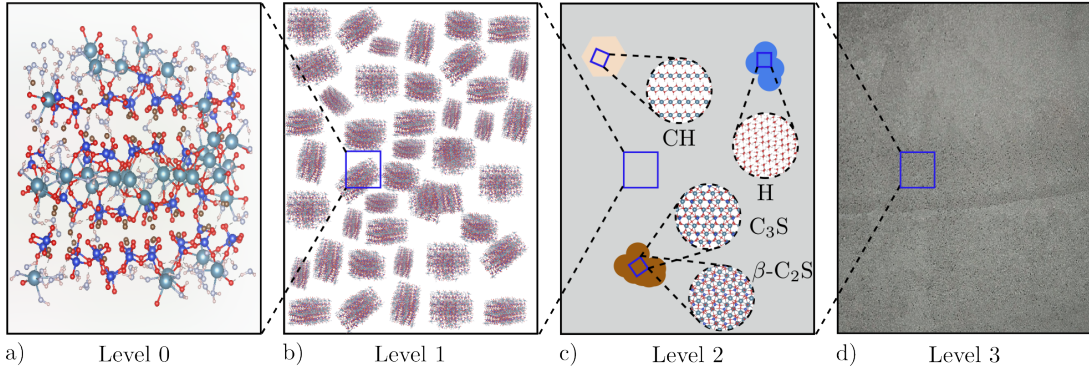


Figure 1.1: A four-level model representing the upscaling of C-S-H properties from the nanoscale to the engineering scale. (a) snapshot of C-S-H's nanostructure. (b) microstructure of C-S-H created by agglomeration of randomly oriented C-S-H nanoparticles. (c) microtexture of hardened paste composed by hydration products. (d) macrotexture of cement paste at the engineering scale. Adapted from⁹.

1.2 Problem Statement

Nunc posuere quam at lectus tristique eu ultrices augue venenatis. Vestibulum ante ipsum primis in faucibus orci luctus et ultrices posuere cubilia Curae; Aliquam erat volutpat. Vivamus sodales tortor eget quam adipiscing in vulputate ante ullamcorper. Sed eros ante, lacinia et sollicitudin et, aliquam sit amet augue. In hac habitasse platea dictumst.

1.3 General and Specific Objectives

Morbi rutrum odio eget arcu adipiscing sodales. Aenean et purus a est pulvinar pellentesque. Cras in elit neque, quis varius elit. Phasellus fringilla, nibh eu tempus venenatis, dolor elit posuere quam, quis adipiscing urna leo nec orci. Sed nec nulla auctor odio aliquet consequat. Ut nec nulla in ante ullamcorper aliquam at sed dolor. Phasellus fermentum magna in augue gravida cursus. Cras sed pretium lorem. Pellentesque eget ornare odio. Proin accumsan, massa viverra cursus pharetra, ipsum nisi lobortis velit, a malesuada dolor lorem eu neque.

1.4 Overview

Sed ullamcorper quam eu nisl interdum at interdum enim egestas. Aliquam placerat justo sed lectus lobortis ut porta nisl porttitor. Vestibulum mi dolor, lacinia molestie gravida at, tempus vitae ligula. Donec eget quam sapien, in viverra eros. Donec pellentesque justo a massa fringilla non vestibulum metus vestibulum. Vestibulum in orci quis felis tempor lacinia. Vivamus ornare ultrices facilisis. Ut hendrerit volutpat vulputate. Morbi condimentum venenatis augue, id porta ipsum vulputate in. Curabitur luctus tempus justo. Vestibulum risus lectus, adipiscing

nec condimentum quis, condimentum nec nisl. Aliquam dictum sagittis velit sed iaculis. Morbi tristique augue sit amet nulla pulvinar id facilisis ligula mollis. Nam elit libero, tincidunt ut aliquam at, molestie in quam. Aenean rhoncus vehicula hendrerit.

Chapter 2

Theoretical Background

This chapter is devoted to present the theoretical foundations and formalism of Density Functional Theory (DFT) and related methods required for the development of the results presented in this work. Starting with the many-body Schrödinger equation, this chapter covers the Born-Oppenheimer approximation, the Hartree-Fock approximation, Hohenberg-Kohn theorems, the Kohn-Sham equations, exchange-correlation functionals, and definitions on Ab initio molecular dynamics (AIMD) and machine learning force fields (MLFFs), along with implementation details in the Vienna Ab initio Simulation Package (VASP).

Ultimately, this chapter aims to provide a comprehensive understanding of the theoretical framework that underpins the computational methods utilised in this work, enabling the reader to grasp the principles and assumptions that govern the simulations and analyses performed throughout.

2.1 Many Body Schrödinger Equation

In our efforts to unravel the tapestry of materials, quantum mechanics lights our path towards describing the complex, yet fundamental interactions that govern particle behaviour at the atomic scale. Our journey shall commence by describing the physical laws that shape the interactions among particles constituting a system—electrons and nuclei alike.

2.1.1 The Coulomb Interaction

Materials may be thought of as complex assemblies of electrons and nuclei, held together by a delicate balance between attractive Coulomb interactions—primarily between electrons and nuclei—and repulsive interactions between like-charged particles, such as electron-electron and

nucleus-nucleus pairs, which govern the overall dynamics of the material system^{10,11,12}. From classical electrostatics, these interactions can be mathematically expressed as follows:

- Electron-electron interactions

$$\hat{V}_{ee} = \frac{1}{2} \sum_{i \neq j} \frac{e^2}{4\pi\epsilon_0 |\mathbf{r}_i - \mathbf{r}_j|} \quad (2.1)$$

- Electron-nucleus interactions

$$\hat{V}_{nn} = \frac{1}{2} \sum_{I \neq J} \frac{e^2}{4\pi\epsilon_0} \frac{Z_I Z_J}{|\mathbf{R}_I - \mathbf{R}_J|} \quad (2.2)$$

- Electron-nuclei interactions

$$\hat{V}_{en} = - \sum_{i \neq I} \frac{e^2}{4\pi\epsilon_0} \frac{Z_I}{|\mathbf{r}_i - \mathbf{R}_I|} \quad (2.3)$$

where e is the electronic charge, ϵ_0 is the vacuum permittivity, Z_I and Z_J are the atomic numbers of nuclei I and J , respectively, and \mathbf{r}_i and \mathbf{R}_I are the position vectors of electrons and nuclei, respectively. Moreover, we must also consider the kinetic energy of the collection of electrons and nuclei

$$\hat{T} = - \sum_i \frac{\hbar^2}{2m_e} \nabla_i^2 - \sum_I \frac{\hbar^2}{2M_I} \nabla_I^2 \quad (2.4)$$

where \hbar is the reduced Planck's constant, m_e is the electron mass, and M_I is the mass of the nucleus I .

2.1.2 The Time-Independent Schrödinger Equation

The Time-Independent Schrödinger Equation (TISE) lies at the heart of non-relativistic quantum mechanics, providing a mathematical framework to describe stationary electronic states of quantum systems. It takes the following form:

$$\hat{H}\psi(\mathbf{r}) = E\psi(\mathbf{r}) \quad (2.5)$$

where \hat{H} is the Hamiltonian of the system, incorporating both the kinetic and potential energies, $\psi(\mathbf{r})$ is an eigenstate of the system, and E is the energy eigenvalue associated with eigenstate $\psi(\mathbf{r})$. It is important to note that Equation 2.5 is only applicable to a single particle, yet a material system is composed of many electrons (N) and nuclei (M) with spatial coordinates

$\mathbf{r}_1, \mathbf{r}_2, \dots, \mathbf{r}_N$ and $\mathbf{R}_1, \mathbf{R}_2, \dots, \mathbf{R}_M$, respectively. Therefore, we must introduce a so-called many-body wavefunction given by:

$$\Psi(\mathbf{r}_1, \mathbf{r}_2, \dots, \mathbf{r}_N, \mathbf{R}_1, \mathbf{R}_2, \dots, \mathbf{R}_M) \quad (2.6)$$

On this basis, the many-body version of Equation 2.5 shall be constructed by combining the kinetic (Equation 2.4) and potential (Equations 2.1, 2.2, and 2.3) energy contributions, leading to the following expression:

$$\left[-\sum_i \frac{\hbar^2}{2m_e} \nabla_i^2 - \sum_I \frac{\hbar^2}{2M_I} \nabla_I^2 + \frac{1}{2} \sum_{i \neq j} \frac{e^2}{4\pi\epsilon_0 |\mathbf{r}_i - \mathbf{r}_j|} + \frac{1}{2} \sum_{I \neq J} \frac{e^2}{4\pi\epsilon_0} \frac{Z_I Z_J}{|\mathbf{R}_I - \mathbf{R}_J|} - \sum_{i,I} \frac{e^2}{4\pi\epsilon_0} \frac{Z_I}{|\mathbf{r}_i - \mathbf{R}_I|} \right] \Psi = E_{\text{tot}} \Psi \quad (2.7)$$

Equation 2.7 provides a complete description of the stationary states of a non-relativistic many-body system, under time-independent conditions and in the absence of external fields. Additionally, we can achieve a more compact formulation by introducing the concept of atomic units. To this end, let us consider the simplest electron-nucleus system—the hydrogen atom—where the electron orbital has an average radius $a_0 \approx 0.529 \text{ \AA}$. Thereby, the Coulomb energy for such a system is given by:

$$E_{\text{Ha}} = \frac{e^2}{4\pi\epsilon_0 a_0} \quad (2.8)$$

where 'Ha' stands for Hartree. Within this framework, the Hartree energy represents the Coulomb interaction between two fundamental charges separated by a distance of one Bohr radius (a_0). Moreover, the angular momentum quantisation condition for the electron in the hydrogen atom is given by

$$m_e v a_0 = \hbar \quad (2.9)$$

Additionally, the equilibrium condition between the nuclear attraction and the electron's centrifugal force can be expressed as:

$$\frac{e^2}{4\pi\epsilon_0 a_0^2} = \frac{m_e v^2}{a_0} \quad (2.10)$$

By combining Equations 2.8, 2.9, and 2.10, we derive the following relationships:

$$\frac{e^2}{4\pi\epsilon_0 a_0} = \frac{\hbar^2}{m_e a_0^2} \quad (2.11)$$

$$\frac{1}{2} m_e v^2 = \frac{1}{2} E_{\text{Ha}} \quad (2.12)$$

This latter relation showcases that the kinetic energy is of the same order as E_{Ha} , rendering it convenient to normalise Equation 2.7 by this quantity:

$$\left[-\sum_i \frac{1}{2} a_0^2 \nabla_i^2 - \sum_I \frac{1}{2} \frac{1}{(M_I/m_e)} \nabla_I^2 + \frac{1}{2} \sum_{i \neq j} \frac{a_0}{|\mathbf{r}_i - \mathbf{r}_j|} + \frac{1}{2} \sum_{I \neq J} Z_I Z_J \frac{a_0}{|\mathbf{R}_I - \mathbf{R}_J|} - \sum_{i,I} Z_I \frac{a_0}{|\mathbf{r}_i - \mathbf{R}_I|} \right] \Psi = \frac{E_{\text{tot}}}{E_{\text{Ha}}} \Psi \quad (2.13)$$

A final simplification involves setting our energy units to Ha, distance units to a_0 , and mass units to m_e . The last missing constant e is set to 1, leading to the following expression:

$$\left[-\sum_i \frac{\nabla_i^2}{2} - \sum_I \frac{\nabla_I^2}{2M_I} + \frac{1}{2} \sum_{i \neq j} \frac{1}{|\mathbf{r}_i - \mathbf{r}_j|} + \frac{1}{2} \sum_{I \neq J} \frac{Z_I Z_J}{|\mathbf{R}_I - \mathbf{R}_J|} - \sum_{i,I} \frac{Z_I}{|\mathbf{r}_i - \mathbf{R}_I|} \right] \Psi = E_{\text{tot}} \Psi \quad (2.14)$$

Ultimately, even though Equation 2.14 provides an exact method capable of yielding various properties of a material system—such as elastic, thermal, and electronic properties—a combination of mathematical complexity and computational limitations renders it intractable to solve for any realistic system. Moreover, the wavefunction contains vastly more information than is necessary to describe most observable properties of a material. Therefore, we must resort to alternative formulations that allow us to extract only the relevant information from the wavefunction whilst reducing the computational cost of the calculations. The remainder of this chapter is dedicated to presenting such alternative approaches that ultimately lead to the computational methods employed throughout this work.

2.2 The Born-Oppenheimer Approximation

For atoms in a solid, we can think of nuclei as being held immobile in a fixed position, while electrons instantaneously react to any nucleus's movement. This assumption is based on the fact that nuclei are much heavier than electrons—by three to four orders of magnitude—making the former behave like classical particles. Thereby, we can rewrite the many-body wavefunction as a product of two wavefunctions:

$$\Psi(\mathbf{r}_1, \mathbf{r}_2, \dots, \mathbf{r}_N, \mathbf{R}_1, \mathbf{R}_2, \dots, \mathbf{R}_M) = \psi_{\mathbf{R}}(\mathbf{r}_1, \mathbf{r}_2, \dots, \mathbf{r}_N) \chi(\mathbf{R}) \quad (2.15)$$

where $\psi_{\mathbf{R}}$ is the electronic wavefunction parametrised by the nuclear positions \mathbf{R} , and χ is the nuclear wavefunction. Furthermore, this significant mass disparity enables a systematic

approximation scheme, wherein the electronic wavefunction is solved for fixed nuclei, and its solution is used as an effective potential for the nuclear dynamics afterwards. First, nuclei' kinetic energy is neglected, as their positions are assumed to be fixed:

$$\sum_I \frac{\nabla_I^2}{2M_I} = 0 \quad \text{and} \quad E = E_{\text{tot}} - \sum_{I < J} \frac{Z_I Z_J}{|\mathbf{R}_I - \mathbf{R}_J|} \quad (2.16)$$

Following, we define the Coulomb potential of the nuclei experienced by the electrons as:

$$V_n(\mathbf{r}) = - \sum_I \frac{Z_I}{|\mathbf{r} - \mathbf{R}_I|} \quad (2.17)$$

Then, Equation 2.14 can be rewritten as:

$$\left[- \sum_i \frac{\nabla_i^2}{2} + \sum_i V_n(\mathbf{r}_i) + \frac{1}{2} \sum_{i \neq j} \frac{1}{|\mathbf{r}_i - \mathbf{r}_j|} \right] \Psi = E\Psi \quad (2.18)$$

Finally, by using Equation 2.15, we can define the electronic and nuclear Schrödinger equations as follows:

$$\left[- \sum_i \frac{\nabla_i^2}{2} + \sum_i V_n(\mathbf{r}_i) + \frac{1}{2} \sum_{i \neq j} \frac{1}{|\mathbf{r}_i - \mathbf{r}_j|} \right] \psi_{\mathbf{R}} = E_{\mathbf{R}} \psi_{\mathbf{R}} \quad (2.19)$$

$$\left[- \sum_I \frac{\nabla_I^2}{2M_I} + \sum_{I < J} \frac{Z_I Z_J}{|\mathbf{R}_I - \mathbf{R}_J|} + E(\mathbf{R}_1, \dots, \mathbf{R}_M) \right] \chi(\mathbf{R}) = E_{\text{tot}} \chi(\mathbf{R}) \quad (2.20)$$

where $E_{\mathbf{R}} = E(\mathbf{R}_1, \dots, \mathbf{R}_M)$ is the electronic surface energy, which is a function of the nuclear positions, and serves as an effective potential shaping the nuclear dynamics.

2.3 Hartree-Fock Approximation

The essence of the Hartree-Fock approximation (HFA) is to approximate the interacting many-electron system (Equation 2.18) by a set of non-interacting single-particle problems subject to an effective mean-field potential^{13,14,15}. As a means to this, we first rewrite the total wavefunction for a system with N electrons as the product of single-electron wavefunctions—often referred to as the Hartree approximation¹⁶—as showcased in Equation 2.21.

$$\Psi^H(\mathbf{r}_1, \dots, \mathbf{r}_N) = \prod_{i=1}^N \phi_i(\mathbf{r}_i) \quad (2.21)$$

Following, we construct the total energy functional as the expectation value of the Hamiltonian operator:

$$E^H[\{\phi_i\}] = \left\langle \Psi^H \middle| \hat{H} \middle| \Psi^H \right\rangle \quad (2.22)$$

Expanding Equation 2.22:

$$E^H[\{\phi_i\}] = \sum_{i=1}^N \int \phi_i^*(\mathbf{r}) \left(-\frac{\nabla^2}{2} + V_n(\mathbf{r}) \right) \phi_i(\mathbf{r}) d\mathbf{r} + \frac{1}{2} \sum_{i \neq j} \int \int \frac{|\phi_i(\mathbf{r})|^2 |\phi_j(\mathbf{r}')|^2}{|\mathbf{r} - \mathbf{r}'|} d\mathbf{r} d\mathbf{r}' \quad (2.23)$$

where the first term adds up the kinetic energy and electron-nuclear attraction overall electrons, whilst the second accounts for the classical electron-electron repulsion energy averaged over the electron density distribution. In order to find the set of orbitals $\{\phi_i\}$ that minimises the total energy functional, we use the variational principle, where we shall impose the orthonormality condition:

$$\int \phi_i^*(\mathbf{r}) \phi_j(\mathbf{r}) d\mathbf{r} = \delta_{ij} \quad (2.24)$$

for what we introduce the Lagrange multipliers λ_{ij} to enforce these constraints and define the Lagrangian:

$$\mathcal{L} = E^H[\{\phi_i\}] - \sum_{i=1}^N \lambda_{ij} (\langle \phi_i | \phi_j \rangle - \delta_{ij}) \quad (2.25)$$

which ultimately simplifies to:

$$\mathcal{L} = E^H[\{\phi_i\}] - \sum_{i=1}^N \varepsilon_i (\langle \phi_i | \phi_i \rangle - 1) \quad (2.26)$$

Then, we need to compute the derivative of \mathcal{L} with respect to ϕ_i^* and set it to zero:

$$\frac{\delta \mathcal{L}}{\delta \phi_i^*}(\mathbf{r}) = 0 \quad (2.27)$$

which yields the Hartree equation:

$$\left[-\frac{\nabla^2}{2} + V_n(\mathbf{r}) + V_i^H(\mathbf{r}) \right] \phi_i(\mathbf{r}) = \varepsilon_i \phi_i(\mathbf{r}) \quad (2.28)$$

where $V_n(\mathbf{r})$ represents the electrostatic interaction between electrons and nuclei, and the Hartree potential

$$V_i^H(\mathbf{r}) = \sum_{j \neq i} \int \frac{|\phi_j(\mathbf{r}')|^2}{|\mathbf{r} - \mathbf{r}'|} d\mathbf{r}' \quad (2.29)$$

accounts for the average electrostatic interaction experienced by the i -th electron due to all other electrons in the system. This effective mean-field potential replaces the electron-electron interactions, effectively simplifying the many-body problem into single-particle problems.

2.3.1 The Pauli Exclusion Principle

So far, we have introduced the Hartree approximation, which assumes that the many-electron wavefunction can be expressed as a product of single-particle wavefunctions. However, this approach does not account for the indistinguishability of electrons and the Pauli exclusion principle, which states that no two fermions—half-spin particles, such as electrons—can reside in the same quantum state simultaneously. In doing so, it imposes a restriction on the possible configurations of electrons in a system that shall be accounted for.

In order to achieve this, V. Fock¹⁷ introduced a different approximation to the wavefunction by using a Slater determinant—a mathematical construct that combines one-electron wavefunctions in such a way that satisfies the antisymmetry principle. This is done by expressing the overall wavefunction as the determinant of a matrix of single-electron wavefunctions:

$$\Psi^{HF}(\mathbf{r}_1, \dots, \mathbf{r}_N) = \frac{1}{\sqrt{N!}} \begin{vmatrix} \phi_1(\mathbf{r}_1) & \phi_1(\mathbf{r}_2) & \dots & \phi_1(\mathbf{r}_N) \\ \phi_2(\mathbf{r}_1) & \phi_2(\mathbf{r}_2) & \dots & \phi_2(\mathbf{r}_N) \\ \vdots & \vdots & \ddots & \vdots \\ \phi_N(\mathbf{r}_1) & \phi_N(\mathbf{r}_2) & \dots & \phi_N(\mathbf{r}_N) \end{vmatrix} \quad (2.30)$$

where $1/\sqrt{N!}$ is a normalisation factor. To illustrate this, consider a two-electron system with single-particle wavefunctions $\phi_1(\mathbf{r})$ and $\phi_2(\mathbf{r})$. The Slater determinant for this system would be:

$$\Psi^{HF}(\mathbf{r}_1, \mathbf{r}_2) = \frac{1}{\sqrt{2}} \begin{vmatrix} \phi_1(\mathbf{r}_1) & \phi_1(\mathbf{r}_2) \\ \phi_2(\mathbf{r}_1) & \phi_2(\mathbf{r}_2) \end{vmatrix} = \frac{1}{\sqrt{2}} [\phi_1(\mathbf{r}_1)\phi_2(\mathbf{r}_2) - \phi_1(\mathbf{r}_2)\phi_2(\mathbf{r}_1)] \quad (2.31)$$

Evidently, $\Psi^{HF}(\mathbf{r}_1, \mathbf{r}_2) = -\Psi^{HF}(\mathbf{r}_2, \mathbf{r}_1)$, which satisfies the antisymmetr principle.

2.3.2 The Hartree-Fock Equations

The Hartree-Fock equations are derived in a similar manner we addressed the Hartree equations. We first define the total energy with the Hartree-Fock wavefunction (Equation 2.30)

$$\begin{aligned} E^{HF}[\{\phi_i\}] &= \left\langle \Psi^{HF} \left| \hat{H} \right| \Psi^{HF} \right\rangle \\ &= \sum_i \langle \phi_i | \frac{\nabla^2}{2} + V_n(\mathbf{r}) | \phi_i \rangle \\ &\quad + \frac{1}{2} \sum_{i \neq j} \langle \phi_i \phi_j | \frac{1}{|\mathbf{r}_i - \mathbf{r}_j|} | \phi_i \phi_j \rangle \\ &\quad - \frac{1}{2} \sum_{i \neq j} \langle \phi_i \phi_j | \frac{1}{|\mathbf{r}_i - \mathbf{r}_j|} | \phi_j \phi_i \rangle \end{aligned} \quad (2.32)$$

Consequently, using the variational principle, we derive the Hartree-Fock equations:

$$\left[-\frac{\nabla^2}{2} + V_n(\mathbf{r}) + V_i^H(\mathbf{r}) + \right] \phi_i(\mathbf{r}) - \sum_{j \neq i} \langle \phi_j | \frac{1}{|\mathbf{r}_i - \mathbf{r}_j|} | \phi_i \rangle \phi_j(\mathbf{r}) = \varepsilon_i \phi_i(\mathbf{r}) \quad (2.33)$$

Noticeably, Equation 2.33 has an extra term compared with the Hartree equation (Equation 2.28). This term is called the "exchange" term¹², and describes the effects of exchange between electrons. It is convenient to try to express the Hartree-Fock equations in a more compact form, so we define the single-particle and total densities as

$$\rho_i(\mathbf{r}) = |\phi_i(\mathbf{r})|^2 \quad (2.34)$$

$$\rho(\mathbf{r}) = \sum_i \rho_i(\mathbf{r}) \quad (2.35)$$

so the Hartree potential can be expressed as

$$V_i^H(\mathbf{r}) = \sum_{j \neq i} \int \frac{\rho_j(\mathbf{r}')}{|\mathbf{r} - \mathbf{r}'|} d\mathbf{r}' = \int \frac{\rho(\mathbf{r}') - \rho_i(\mathbf{r}')}{|\mathbf{r} - \mathbf{r}'|} d\mathbf{r}' \quad (2.36)$$

Therefore, the single-particle exchange density can be constructed as

$$\rho_i^X(\mathbf{r}, \mathbf{r}') = \sum_{j \neq i} \frac{\phi_i(\mathbf{r}') \phi_i^*(\mathbf{r}) \phi_j(\mathbf{r}) \phi_j^*(\mathbf{r}')}{\phi_i(\mathbf{r}) \phi_i^*(\mathbf{r})} \quad (2.37)$$

Finally, the Hartree-Fock equations take the form

$$\left[-\frac{\nabla^2}{2} + V_n(\mathbf{r}) + V_i^H(\mathbf{r}) + V_i^X(\mathbf{r}) \right] \phi_i(\mathbf{r}) = \varepsilon_i \phi_i(\mathbf{r}) \quad (2.38)$$

where V_i^X stands for the exchange potential

$$V_i^X(\mathbf{r}) = - \int \frac{\rho_i^X(\mathbf{r}, \mathbf{r}')}{|\mathbf{r} - \mathbf{r}'|} d\mathbf{r}' \quad (2.39)$$

2.4 Density Functional Theory

So far, we have acknowledged that determining the state of a system with N electrons remains a formidable challenge, for it involves a wavefunction defined in a $3N$ -dimensional space. We also recognise that it is possible—heuristically speaking—to simplify such representation by utilising products of single-particle wavefunctions. Nevertheless, such an independent electron approximation necessitates the wavefunctions to be explicitly specified, thereby yielding a rather drastic approximation for the behaviour of the system. Thus, it is natural to consider a different

approach to develop the appropriate single-particle framework in an exact manner, onto which approximations can be introduced afterwards.

We hereby introduce the Density Functional Theory (DFT), which draws upon the insight that any property of a system of many electrons can be viewed as a functional of the ground-state density $n(\mathbf{r})$ ¹⁸ (Equation 2.40)—a scalar function defined over three spatial coordinates.

$$n(\mathbf{r}) = N \int \Psi^*(\mathbf{r}, \dots, \mathbf{r}_N) \Psi(\mathbf{r}, \dots, \mathbf{r}_N) d\mathbf{r}_2 \dots d\mathbf{r}_N \quad (2.40)$$

The foundational principles of DFT were established in the original papers by Hohenberg, Kohn and Sham^{19,20}, where they present two theorems that establish the theoretical framework of DFT. However, for the purposes of this discussion, we shall base our exposition on explanatory texts^{18,10,12,11}.

2.4.1 First Hohenberg-Kohn Theorem

Theorem 2.1 (First Hohenberg-Kohn Theorem). *The ground-state electron density $n(\mathbf{r})$ uniquely determines the external potential $V(\mathbf{r})$ and, consequently, the ground-state energy E_0 of a many-electron system.*

Proof. Suppose two different external potentials, $V(\mathbf{r})$ and $V'(\mathbf{r})$ (different ionic potentials) yield the same ground-state electron density $n(\mathbf{r})$. Given that $V(\mathbf{r})$ and $V'(\mathbf{r})$ are different in a non-trivial way, we will show that this statement leads to a contradiction. Let E and Ψ be the total energy and wavefunction and E' and Ψ' be the total energy and wavefunction corresponding to the systems with hamiltonians \hat{H} and \hat{H}' , respectively, with the first hamiltonian containing $V(\mathbf{r})$ and the second containing $V'(\mathbf{r})$ as an external potential:

$$\hat{H} = \hat{T} + \hat{U} + V, \quad \hat{H}' = \hat{T} + \hat{U} + V', \quad E = \langle \Psi | \hat{H} | \Psi \rangle, \quad E' = \langle \Psi' | \hat{H}' | \Psi' \rangle$$

Here, \hat{T} and \hat{U} correspond to the kinetic and interaction energy operators, thereby being common for both Hamiltonians. Now, we assume that the ground states of the two Hamiltonians are different because the external potentials are different. Then, according to the variational principle:

$$\begin{aligned} E < \langle \Psi' | \hat{H} | \Psi' \rangle &= \langle \Psi' | \hat{T} + \hat{U} + V + V' - V' | \Psi' \rangle \\ &= \langle \Psi' | \hat{H}' + V - V' | \Psi' \rangle \\ &= E' + \langle \Psi' | (V - V') | \Psi' \rangle \end{aligned} \quad (2.41)$$

Following the same reasoning, we can prove that

$$E' < E - \langle \Psi | (V - V') | \Psi \rangle \quad (2.42)$$

Adding Equations 2.41 and 2.42, we obtain:

$$E + E' < E' + E - \langle \Psi | (V - V') | \Psi \rangle + \langle \Psi' | (V - V') | \Psi' \rangle \quad (2.43)$$

where the last two terms result in

$$\int n'(\mathbf{r})(V - V')d\mathbf{r} - \int n(\mathbf{r})(V - V')d\mathbf{r} = 0 \quad (2.44)$$

since $n(\mathbf{r}) = n'(\mathbf{r})$ by assumption. Finally, we arrive at the following expression:

$$E + E' < E + E' \quad (2.45)$$

Evidently, this is a contradiction, which implies that our initial assumption about the densities being the same ought to be false, thereby proving there is a one-to-one correspondence between an external potential $V(\mathbf{r})$ and the electron density $n(\mathbf{r})$. Moreover, since $V(\mathbf{r})$ determines the wavefunction, the wavefunction must be a unique functional of the density. So we conclude that the expression

$$\mathcal{F}[n(\mathbf{r})] = \langle \Psi | \hat{T} + \hat{U} | \Psi \rangle \quad (2.46)$$

must be a universal functional of the electronic density—*i.e.*, common to all solids—and that the ground state energy is a functional of the density:

$$E[n(\mathbf{r})] = \mathcal{F}[n(\mathbf{r})] + \int V(\mathbf{r})n(\mathbf{r})d\mathbf{r} \quad (2.47)$$

□

2.4.2 Second Hohenberg-Kohn Theorem

Theorem 2.2 (Second Hohenberg-Kohn Theorem). *The ground-state energy E can be obtained through the variation of trial densities $\tilde{n}(\mathbf{r})$ instead of trial wavefunctions $\tilde{\Psi}$.*

Proof. First, we fix a trial density $\tilde{n}(\mathbf{r})$ and define the trial wavefunctions $\tilde{\Psi}_{\tilde{n}(\mathbf{r})}^\alpha$. Therefore, the constrained energy minimum is defined as

$$\begin{aligned} E[\tilde{n}(\mathbf{r})] &= \min_\alpha \langle \tilde{\Psi}_{\tilde{n}(\mathbf{r})}^\alpha | \hat{H} | \tilde{\Psi}_{\tilde{n}(\mathbf{r})}^\alpha \rangle \\ &= \mathcal{F}[\tilde{n}(\mathbf{r})] + \int V(\mathbf{r})\tilde{n}(\mathbf{r})d\mathbf{r} \end{aligned} \quad (2.48)$$

Secondly, we minimise Equation 2.48 over all n

$$E = \min_{\tilde{n}(\mathbf{r})} E[\tilde{n}(\mathbf{r})] = \min_{\tilde{n}(\mathbf{r})} \left\{ \mathcal{F}[\tilde{n}(\mathbf{r})] + \int V(\mathbf{r})\tilde{n}(\mathbf{r})d\mathbf{r} \right\} \quad (2.49)$$

For a non-degenerate ground state, the minimum corresponds to the ground-state $n(\mathbf{r})$, or to one of the ground-state densities otherwise. \square

Finally, we have managed to map the formidable challenge of finding the minimum of $\langle \Psi | \hat{H} | \Psi \rangle$ involving a $3N$ -dimensional wavefunction into a much simpler problem of finding the minimum of $E[n(\mathbf{r})]$ involving a 3-dimensional function. This is the essence of DFT, which allows us to compute the ground-state properties of many-electron systems without explicitly solving the many-body Schrödinger equation.

2.4.3 Kohn-Sham Equations

Even though the Hohenberg-Kohn theorems provide a rigorous foundation for DFT, they offer no guidance whatsoever for constructing the functional $\mathcal{F}[n(\mathbf{r})]$. As such, density functional theory would lack practical utility if it were not for the auxiliary system proposed by Kohn and Sham¹⁸. It consists of replacing the many-electron problem by an auxiliary independent-particle problem that yields the same ground-state density, incorporating the many-body effects into a so-called exchange-correlation functional. To this end, we first define the density of the auxiliary system as

$$n(\mathbf{r}) = \sum_i |\phi_i(\mathbf{r})|^2 \quad (2.50)$$

where $\phi_i(\mathbf{r})$ are the single-particle wavefunctions of the auxiliary system. Next, we define the independent-particle kinetic energy functional as

$$T_s[n(\mathbf{r})] = \frac{1}{2} \sum_i \int \phi_i^*(\mathbf{r})(-\nabla^2)\phi_i(\mathbf{r}) d\mathbf{r} \quad (2.51)$$

and the Hartree energy functional can be redefined as

$$E_H[n(\mathbf{r})] = \frac{1}{2} \int \frac{n(\mathbf{r})n(\mathbf{r}')}{|\mathbf{r} - \mathbf{r}'|} d\mathbf{r} d\mathbf{r}' \quad (2.52)$$

yielding the following expression for the total energy functional:

$$E^{\text{KS}}[n(\mathbf{r})] = T_s[n(\mathbf{r})] + \int V_{\text{n}}(\mathbf{r})n(\mathbf{r}) d\mathbf{r} + E_H[n(\mathbf{r})] + E_{xc}[n(\mathbf{r})] \quad (2.53)$$

where $E_{xc}[n(\mathbf{r})]$ is the exchange-correlation energy functional is defined as

$$E_{xc}[n(\mathbf{r})] = \langle \hat{T} \rangle - T_s[n(\mathbf{r})] + \langle \hat{U} \rangle - E_H[n(\mathbf{r})] \quad (2.54)$$

having $\langle \hat{T} \rangle$ and $\langle \hat{U} \rangle$ being the exact kinetic energy and electron-electron interaction energy. Finally, we choose a variation in the density to be

$$\delta n(\mathbf{r}) = \delta\phi_i^*(\mathbf{r})\phi_i(\mathbf{r}) \quad (2.55)$$

along with the following constraint

$$\int \delta n(\mathbf{r}) d\mathbf{r} = \int \delta\phi_i^*(\mathbf{r})\phi_i(\mathbf{r}) d\mathbf{r} = 0 \quad (2.56)$$

and by applying the Kohn-Sham variational principle, we arrive at the Kohn-Sham equations:

$$\left[-\frac{\nabla^2}{2} + V_{\text{ext}}(\mathbf{r}) + V_H(\mathbf{r}) + V_{xc}(\mathbf{r}) \right] \phi_i(\mathbf{r}) = \varepsilon_i \phi_i(\mathbf{r}) \quad (2.57)$$

where $V_{\text{ext}}(\mathbf{r})$ is the external potential, $V_H(\mathbf{r})$ is the Hartree potential, and $V_{xc}(\mathbf{r})$ is the exchange-correlation potential defined as

$$V_{xc}(\mathbf{r}) = \frac{\delta E_{xc}[n(\mathbf{r})]}{\delta n(\mathbf{r})} \quad (2.58)$$

Our task now shall focus on constructing appropriate approximations for the exchange-correlation functional $E_{xc}[n(\mathbf{r})]$.

2.4.4 Exchange-Correlation Functionals

The usefulness of DFT relies entirely on whether reliable approximations for the exchange-correlation functional $E_{xc}[n(\mathbf{r})]$ can be constructed with sufficient accuracy and computational efficiency. Therefore, we shall now present the most commonly used approximations for $E_{xc}[n(\mathbf{r})]$, as well as their strengths and weaknesses.

2.4.4.1 Local Density Approximation

The simplest—and remarkably effective—approximation for the exchange-correlation functional is the local-density approximation (LDA)²¹. It approximates the exchange-correlation energy of an inhomogeneous electron system by that of a homogeneous electron gas (HEG) having the same electron density.

$$E_{xc}^{LDA}[n(\mathbf{r})] = \int n(\mathbf{r}) \epsilon_{xc}(n(\mathbf{r})) d\mathbf{r} \quad (2.59)$$

where $\epsilon_{xc}(n)$ is the exchange and correlation energy per electron of a uniform electron gas of density n ^{19,20}. This quantity depends solely on the local density and surrounding electrons in the vicinity of \mathbf{r} , for example, a sphere of radius $\sim \lambda_F(\mathbf{r})$ —the local Fermi wavelength¹⁵ $\lambda_F(\mathbf{r}) \equiv [3\pi^2 n(\mathbf{r})]^{-1/3}$.

The exchange and correlation contributions to E_{xc}^{LDA} can be separated into two terms

$$E_{xc}^{LDA}[n(\mathbf{r})] = E_x^{HEG}[n(\mathbf{r})] + E_c^{HEG}[n(\mathbf{r})] \quad (2.60)$$

The first term corresponds to the exchange energy density contribution

$$\begin{aligned} \epsilon_x^{HEG}(n) &= -\frac{3}{4} \left(\frac{3}{\pi} \right)^{1/3} n^{1/3} \\ &= -\frac{0.458128}{r_s} \end{aligned} \quad (2.61)$$

where r_s is the Wigner-Seitz radius—the radius of a sphere containing one electron and given by $(4\pi/3)r_s^3 = n^{-1}$.

The second term corresponds to the correlation energy, which was computed by Ceperley and Alder²² using quantum Monte Carlo methods. Subsequently, the extracted data was parameterised by Perdew and Zunger²³, yielding the following expression:

$$\epsilon_c^{HEG}(r_s) = \begin{cases} 0.0311 \ln r_s - 0.0480 + 0.002r_s \ln r_s - 0.0116r_s & r_s < 1 \\ -0.1423 & r_s \geq 1 \end{cases} \quad (2.62)$$

LDA has demonstrated remarkable success for most applications involving systems with slowly varying densities or systems with high densities. Nevertheless, LDA—and its spin-polarised version (LSDA)—breaks down in systems governed by strong correlation effects that it loses any resemblance to non-interacting electron gases.

2.4.4.2 Generalised Gradient Approximation

In contrast to LDA—which considers the electronic density to be locally uniform—the generalised gradient approximation (GGA) systematically improves upon LDA by incorporating not only the local density $n(\mathbf{r})$, but also its gradient $\nabla n(\mathbf{r})$, thereby accounting for the inhomogeneities in the electron distribution.

Within this framework, the exchange-correlation energy functional is expressed as a function of the local density and its gradient

$$E_{xc}^{GGA}[n(\mathbf{r})] = \int n(\mathbf{r}) \epsilon_{xc}^{HEG}(n(\mathbf{r})) f(n_\uparrow(\mathbf{r}), n_\downarrow(\mathbf{r}), \nabla n_\uparrow(\mathbf{r}), \nabla n_\downarrow(\mathbf{r})) d\mathbf{r} \quad (2.63)$$

where $n_\uparrow(\mathbf{r})$ is the spin-up electron density and $n_\downarrow(\mathbf{r})$ is the corresponding spin-down density. Additionally, the exact form of f —a parametrised analytic function—depends on the GGA under consideration.

In this regard, one of the most prominent and widely adopted GGA functionals is the Perdew-Burke-Ernzerhof (PBE)²⁴ functional, which was proposed as a solution for the drawbacks of previously proposed GGAs, such as the Perdew-Wang (PW91) functional. Within PBE, all parameters—other than those in $\epsilon_{xc}^{HEG}(n(\mathbf{r}))$ —are fundamental constants. Consequently, the exchange energy term in the PBE functional is given by

$$E_x^{PBE} = \int n(\mathbf{r}) \epsilon_x^{HEG}(n(\mathbf{r})) \left[1 + \kappa - \frac{\kappa}{1 + \mu s^2/\kappa} \right] d\mathbf{r} \quad (2.64)$$

where $\kappa = 0.804$ and $\mu = 0.219$ are the parameters of the PBE functional, $k_F = (3\pi^2 n(\mathbf{r}))^{1/3}$ is the local Fermi wavevector and $s = |\nabla n(\mathbf{r})|/(2k_F n(\mathbf{r}))$ is a dimensionless density gradient.

The correlation energy term in the PBE functional is expressed as

$$E_c^{PBE} = \int n(\mathbf{r}) \left[\epsilon_c^{HEG} + \gamma \phi^3 \ln \left\{ 1 + \frac{\beta}{\gamma} t^2 \left[\frac{1 + At^2}{1 + At^2 + A^2 t^4} \right] \right\} \right] d\mathbf{r} \quad (2.65)$$

where $\gamma = 0.031091$, $\beta = 0.066725$, ϕ is a spin-scaling factor, and A and t are defined as

$$A = \frac{\beta}{\gamma} \left[\exp \left\{ \frac{-\epsilon_c^{HEG}}{\gamma \phi^3} \right\} - 1 \right]^{-1}, \quad t(\mathbf{r}) = \frac{|\nabla n(\mathbf{r})|}{2\phi k_s n(\mathbf{r})} \quad (2.66)$$

where $k_s = \sqrt{4k_F/\pi}$ is the Thomas-Fermi screening wavenumber.

Even though PBE holds a significant advantage over LDA in terms of accuracy, it is not exempt from certain limitations and shortcomings. PBE tends to overestimate equilibrium lattice constants by about 1%—LDA underestimates them by the same amount—which is detrimental for accurate calculations of other equilibrium properties, such as bulk moduli, phonon frequencies and magnetism.

To address this issue, a revised version of the PBE—the PBEsol functional²⁵—was developed, which improves equilibrium properties of densely-packed solids and their surfaces, reducing the overestimation of lattice constants by a factor of ~ 4 . Nonetheless, PBEsol does not perform well for semiconductors and can lead to less accurate total energy calculations compared to PBE. Ultimately, the choice of GGA functional depends on the specific system and properties being investigated, as well as the desired balance between accuracy and computational efficiency.

2.4.4.3 Hybrid Functionals

Functionals mentioned above and their inherent limitations motivated the exploration of hybrid functionals. They offer improved accuracy by incorporating a fraction of the exact nonlocal Hartree-Fock exchange energy into the exchange-correlation functional, allowing efficient yet accurate calculations.

One of these functionals includes PBE0²⁶—a combination of the PBE functional and the exact Hartree-Fock exchange energy. It is defined as

$$E_{xc}^{PBE0} = \frac{1}{4}E_x^{HF} + \frac{3}{4}E_x^{PBE} + E_c^{PBE} \quad (2.67)$$

Another prominent example is the HSE (Heyd-Scuseria-Ernzerhof) functional²⁷, which splits the exchange energy into short-range (SR) and long-range (LR) contributions

$$E_{xc}^{HSE06} = \frac{1}{4}E_x^{HF,SR}(\omega) + \frac{3}{4}E_x^{PBE,SR}(\omega) + E_c^{PBE,LR}(\omega) + E_c^{PBE}(\omega) \quad (2.68)$$

where ω is an adjustable parameter that controls the short and long-range separation in the decomposed Coulomb operator

$$\frac{1}{r} = SR_\omega(\mathbf{r}) + LR_\omega(\mathbf{r}) = \frac{\text{erfc}(\omega r)}{r} + \frac{\text{erf}(\omega r)}{r} \quad (2.69)$$

Ultimately, hybrid functionals provide a considerable improvement in the accuracy of electronic structure calculations over LDA and GGA. Nonetheless, this advantage comes at a higher computational cost. This hierarchy of exchange-correlation functionals is better summarised in the so-called Jacob's ladder²⁸ (Figure 2.1), depicting the trade-off between accuracy and computational cost as we ascend the ladder towards more sophisticated functionals.

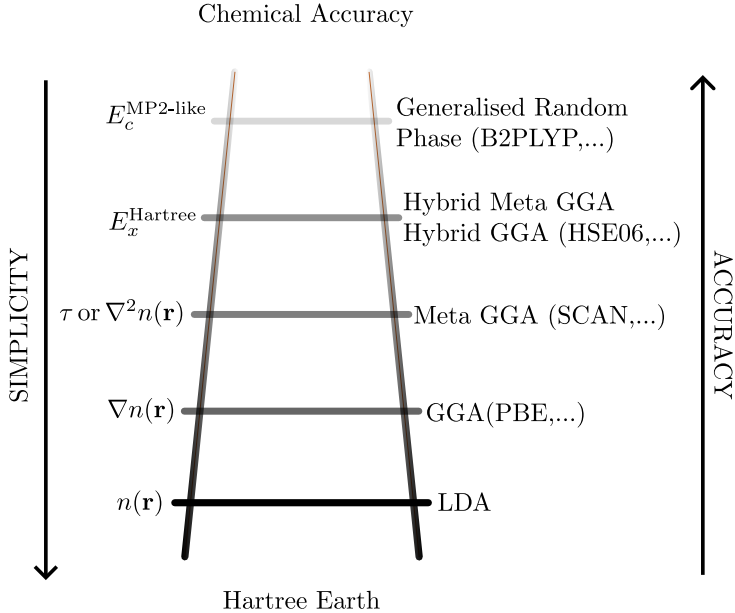


Figure 2.1: Jacob's ladder of exchange-correlation functionals as proposed by J. Perdew²⁸. The ladder categorises the functionals into rungs, from the simplest approximation (LDA) at the bottom, progressing to more sophisticated and accurate approximations (Generalised Random Phase) at the uppermost rung.

2.5 Ab initio Molecular Dynamics

Molecular dynamics (MD)^{29,30} is a widely used computational method, which allows us to simulate a many-body condensed matter system and to compute its thermodynamic and dynamical properties. In MD, a system is modelled as a collection of particles—atoms or molecules—whose trajectories evolve under the influence of interatomic forces following Newton’s equations of motion.

One of the most challenging, yet crucial, aspects of MD is the calculation of the interatomic forces. In classical MD, these forces are typically computed using predefined potential functions or force fields, either constructed upon empirical data or from independent electronic structure calculations that have been parameterised to reproduce experimental or *ab initio* data for small reference systems. Despite their fair success—which we acknowledge but shall not discuss in detail—these empirical interatomic potentials are often limited in their accuracy and transferability. Certain atoms, molecules, or even large systems may give rise to extremely complex interatomic interactions that, if attempted to be modelled with empirical potentials, would demand a rather significant amount of effort. Likewise, these potentials are very often limited to a narrow range of configurations, making them ill-suited for processes involving significant structural changes, such as phase transitions or large deformations.

Therewith, classical MD can be extended by a first-principles approach, where the interatomic forces are computed on-the-fly from accurate electronic structure calculations, ultimately leading to *ab initio* molecular dynamics (AIMD). This approach allows us to overcome the outlined limitations of classical MD, albeit at a significant computational cost. AIMD employs electronic structure methods such as DFT to compute the interatomic forces at each time step, without relying on predefined interatomic potentials, providing AIMD with an improved predictive power and flexibility.

2.5.1 Hellmann-Feynman Theorem

The Hellmann-Feynman theorem^{31,32} establishes a relation between the derivative of the total energy E of a system with respect to a parameter λ and the expectation value of the derivative of the Hamiltonian with respect to that same parameter. While the proof of this theorem is rather straightforward—as shown later in this section—it plays a pivotal role in computing interatomic forces in AIMD.

To this end, let us consider the total energy of a system

$$E = \langle \Psi | \hat{H} | \Psi \rangle \quad (2.70)$$

If λ is a parameter that appears explicitly in the Hamiltonian, then

$$\begin{aligned}\frac{\partial E}{\partial \lambda} &= \frac{\partial}{\partial \lambda} \langle \Psi | \hat{H} | \Psi \rangle \\ &= \left\langle \Psi \left| \frac{\partial \hat{H}}{\partial \lambda} \right| \Psi \right\rangle + \left\langle \frac{\partial \Psi}{\partial \lambda} \left| \hat{H} \right| \Psi \right\rangle + \left\langle \Psi \left| \hat{H} \right| \frac{\partial \Psi}{\partial \lambda} \right\rangle\end{aligned}\quad (2.71)$$

Provided that \hat{H} is hermitian and Ψ is an eigenstate of the hamiltonian, $\hat{H}|\Psi\rangle = E|\Psi\rangle$, Equation 2.71 simplifies to

$$\begin{aligned}\frac{\partial E}{\partial \lambda} &= \left\langle \Psi \left| \frac{\partial \hat{H}}{\partial \lambda} \right| \Psi \right\rangle + \left\langle \frac{\partial \Psi}{\partial \lambda} \left| \hat{H} \right| \Psi \right\rangle + \left\langle \frac{\partial \Psi}{\partial \lambda} \left| \hat{H} \right| \Psi \right\rangle \\ &= \left\langle \Psi \left| \frac{\partial \hat{H}}{\partial \lambda} \right| \Psi \right\rangle + E \frac{\partial}{\partial \lambda} \langle \Psi | \Psi \rangle + E \frac{\partial}{\partial \lambda} \langle \Psi | \Psi \rangle\end{aligned}\quad (2.72)$$

where the last two terms add up to zero, so that Equation 2.72 becomes,

$$\frac{\partial E}{\partial \lambda} = \left\langle \Psi \left| \frac{\partial \hat{H}}{\partial \lambda} \right| \Psi \right\rangle \quad (2.73)$$

yielding the Hellmann-Feynman theorem.

When λ corresponds to the position of a nucleus, the negative derivative of the total energy with respect to λ results in the force acting on that nucleus. More generally, the force on nucleus I can be expressed as the negative gradient of the total energy with respect to its position R_I ,

$$\mathbf{F}_I = -\nabla_{R_I} \langle \Psi | \hat{H} | \Psi \rangle \quad (2.74)$$

This result—referred to as the Hellmann-Feynman force—provides a fundamental connection between the quantum mechanical energy landscape and the classical nuclei motion in AIMD.

2.5.2 Born-Oppenheimer Molecular Dynamics

As previously discussed, AIMD relies on solving the static electronic structure problem at each time step, given a set of fixed nuclear positions at a certain instant in time. One approach to achieve this is the so-called Born-Oppenheimer molecular dynamics (BOMD)³⁰, wherein the potential energy $E[\{\psi_i\}; \mathbf{R}]$ is minimised at each time step with respect to the single-electron wavefunctions $\{\psi_i(\mathbf{r})\}$ under the orthonormality constraint $\langle \psi_i(\mathbf{r}) | \psi_j(\mathbf{r}) \rangle = \delta_{ij}$. The result is a potential energy surface on which the nuclei evolve classically.

This leads to the following Lagrangian

$$\mathcal{L}_{\text{BO}}(\{\psi_i\}; \mathbf{R}, \dot{\mathbf{R}}) = \frac{1}{2} \sum_I M_I \dot{\mathbf{R}}_I^2 - \min_{\{\psi_i\}} E[\{\psi_i(\mathbf{r})\}; \mathbf{R}] + \sum_{ij} \lambda_{ij} (\langle \psi_i | \psi_j \rangle - \delta_{ij}) \quad (2.75)$$

where the first term on the right-hand side corresponds to the classical kinetic energy of the nuclei. The second term, $E[\{\psi_i\}; \mathbf{R}] = E^{\text{KS}}[\{\psi_i[n(\mathbf{r})]\}; \mathbf{R}] + E_{II}$, is the total potential energy consisting of the Kohn-Sham ground-state energy and the nuclear-nuclear interaction energy.

By applying the Euler-Lagrange equations to Equation 2.75

$$\begin{aligned} \frac{d}{dt} \frac{\partial \mathcal{L}}{\partial \dot{\mathbf{R}}_I} &= \frac{\partial \mathcal{L}}{\partial \mathbf{R}_I} \\ \frac{d}{dt} \frac{\partial \mathcal{L}}{\partial \langle \dot{\psi}_i |} &= \frac{\partial \mathcal{L}}{\partial \langle \psi_i |} \end{aligned} \quad (2.76)$$

we obtain the equations of motion

$$M_I \ddot{\mathbf{R}}_I = -\nabla_{\mathbf{R}_I} \left[\min_{\{\psi_i\}} E[\{\psi_i(\mathbf{r})\}; \mathbf{R}] \Big|_{\{\langle \psi_i(\mathbf{r}) | \psi_j(\mathbf{r}) \rangle = \delta_{ij}\}} \right] \quad (2.77)$$

$$0 = -\hat{H}^{\text{KS}} |\psi_i\rangle + \sum_j \lambda_{ij} |\psi_j\rangle \quad (2.78)$$

where Equation 2.77 corresponds to the classical Newtonian equations of motion for the nuclei, and Equation 2.78 represents the Kohn-Sham eigenvalue problem.

Finally, AIMD simulations may also include temperature control, which can be achieved by coupling a thermostat to the system in order to simulate different thermodynamic ensembles—*e.g.*, canonical (NVT) or isothermal-isobaric (NPT) ensembles. However, the details of thermostats and different ensembles are beyond the scope of this report, and we shall refer the reader to the literature^{33,34} for a more detailed discussion of these topics.

2.6 Computational Implementation in VASP

The computational studies presented in this report were performed using the Vienna Ab initio Simulation Package (VASP). This is a software suited for performing *ab initio* quantum mechanical calculations³⁵. It employs DFT as the basic method, albeit it also allows for beyond-DFT methods such as hybrid functionals, many-body perturbation theory (the GW method) and random phase approximation (RPA).

VASP is widely adopted in areas such as materials science, condensed matter physics and quantum chemistry, owing to its demonstrated accuracy and state-of-the-art methods. Consequently, this section is devoted to explaining some important aspects of VASP, with great emphasis on the computational methods employed in this work.

2.6.1 Pseudopotentials

An important step towards defining the wavefunctions that describe an atom is the effective modelling of the electron-ion potential. In this context, core electrons represent a challenge since their rapidly oscillating wavefunctions require a denser real-space grid and a larger number of basis functions to be accurately represented.

To circumvent this problem, we first need to consider the fact that core electrons are tightly bound and do not participate in chemical bonding. Therefore, we can treat them as frozen—*i.e.*, keeping them in their ground state and isolated from the solid-state environment—focusing the calculations on valence electrons, as they do participate in chemical bonding and determine the material’s properties. Nonetheless, any adopted approximation must adequately account for the influence of core electrons on the valence states, such as screening and exchange interactions.

To this end, we shall introduce the concept of pseudopotentials³⁶. This approximation aims to describe the valence electrons without explicitly treating the core states, replacing the strong Coulomb potential near the nucleus with a weaker one. We start by splitting the single-electron states into valence and core states, identified as $|\psi_v\rangle$ and $|\psi_c\rangle$, respectively. We then define a new set of valence states $|\tilde{\psi}_v\rangle$ through the following relation

$$|\tilde{\psi}_v\rangle = |\psi_v\rangle + \sum_c |\psi_c\rangle \langle \psi_c | \tilde{\psi}_v \rangle \quad (2.79)$$

Applying the single-particle Hamiltonian H^{sp} to the pseudo-valence states, and taking into account that $|\psi_v\rangle$ and $|\psi_c\rangle$ are eigenstates of the single-particle Hamiltonian, we get

$$\begin{aligned} H^{sp} |\tilde{\psi}_v\rangle &= H^{sp} |\psi_v\rangle + \sum_c H^{sp} |\psi_c\rangle \langle \psi_c | \tilde{\psi}_v \rangle \\ &= \epsilon_v |\psi_v\rangle + \sum_c \epsilon_c |\psi_c\rangle \langle \psi_c | \tilde{\psi}_v \rangle \\ &= \epsilon_v |\psi_v\rangle + \sum_c (\epsilon_c - \epsilon_v) |\psi_c\rangle \langle \psi_c | \tilde{\psi}_v \rangle \end{aligned} \quad (2.80)$$

Rearranging the terms, we obtain the following expression

$$\left[H^{sp} + \sum_c (\epsilon_v - \epsilon_c) |\psi_c\rangle \langle \psi_c | \right] |\tilde{\psi}_v\rangle = \epsilon_v |\tilde{\psi}_v\rangle \quad (2.81)$$

Equation 2.81 describes the Hamiltonian of the pseudo-valence states, which we can define as

$$\hat{H}^{ps} = H^{sp} + \sum_c (\epsilon_v - \epsilon_c) |\psi_c\rangle \langle \psi_c | \quad (2.82)$$

The modified potential for these states is called the pseudopotential, given by

$$V^{ps}(\mathbf{r}) = V^{sp} + \sum_c (\epsilon_v - \epsilon_c) |\psi_c\rangle \langle \psi_c| \quad (2.83)$$

We emphasise that the pseudo-valence states associated with Equation 2.81 has the same single-particle energies as the valence states, and they remain orthogonal to the core states. However, they are not strictly normalised, which can introduce minor inaccuracies in practical calculations.

Various pseudopotentials have been proposed to achieve the desired trade-off between accuracy and computational cost. Those pseudopotentials requiring larger cut-off energies—hard pseudopotentials—are better suited for capturing the strong interactions inherent in core electrons. In contrast, soft pseudopotentials are often preferred as they require fewer basis functions, reducing the computational cost, albeit at the expense of accuracy.

2.6.2 Projector Augmented-Wave (PAW) Method in VASP

The projector augmented wave (PAW) method—implemented in VASP and used in this work—aims to address some limitations of pseudopotentials by introducing auxiliary functions called projectors, allowing for core and valence electrons to be better represented and enhance computational efficiency.

However, before we introduce the PAW formalism—at least to the extent necessary for this report—we shall first introduce some important concepts that underpin the PAW method.

2.6.2.1 Key Concepts

- **Brillouin Zone and k-points**

Crystalline solids are described in real space in terms of a primitive unit cell (PUC)¹², which is the smallest repeating unit capable of generating the entire solid through periodic boundary conditions. It is characterised by a periodic arrangement of lattice points, referred to as the Bravais lattice. All the lattice points are associated with a set of lattice vectors \mathbf{R} formed by all the possible combinations of integer multiples of the primitive lattice vectors \mathbf{a}_1 , \mathbf{a}_2 and \mathbf{a}_3

$$\mathbf{R} = n_1 \mathbf{a}_1 + n_2 \mathbf{a}_2 + n_3 \mathbf{a}_3, \quad n_1, n_2, n_3 \in \mathbb{Z} \quad (2.84)$$

The primitive unit cell is then defined as the volume enclosed by the primitive lattice vectors

$$V_{PUC} = \mathbf{a}_1 \cdot (\mathbf{a}_2 \times \mathbf{a}_3) \quad (2.85)$$

Using this definition, it is possible to represent the entire crystal by modelling solely its unit cell. Additionally, to appropriately describe electronic properties, we must transition to reciprocal space, defined by the reciprocal vectors

$$\mathbf{b}_1 = \frac{2\pi}{V_{PUC}}(\mathbf{a}_2 \times \mathbf{a}_3), \quad \mathbf{b}_2 = \frac{2\pi}{V_{PUC}}(\mathbf{a}_3 \times \mathbf{a}_1), \quad \mathbf{b}_3 = \frac{2\pi}{V_{PUC}}(\mathbf{a}_1 \times \mathbf{a}_2) \quad (2.86)$$

that satisfy the condition $\mathbf{a}_i \cdot \mathbf{b}_j = 2\pi\delta_{ij}$. Any reciprocal lattice vector \mathbf{G} can then be expressed as

$$\mathbf{G} = m_1\mathbf{b}_1 + m_2\mathbf{b}_2 + m_3\mathbf{b}_3, \quad m_1, m_2, m_3 \in \mathbb{Z} \quad (2.87)$$

The reciprocal space is divided into regions called Brillouin zones (BZs). The first Brillouin zone is defined as the region in reciprocal space closest to the origin (Γ point). Moreover, the volume of the first BZ is given by

$$V_{BZ} = \frac{(2\pi)^3}{V_{PUC}} \quad (2.88)$$

which ensures consistency between the real and reciprocal spaces, and proper normalisation when integrating physical quantities over the BZ.

Finally, because electrons in a crystal are subjected to a periodic potential, single-electron wavefunctions follow Bloch's theorem and can be expressed as

$$\psi_{\mathbf{k}} = e^{i\mathbf{k}\cdot\mathbf{r}} u_{\mathbf{k}}(\mathbf{r}) \quad (2.89)$$

where \mathbf{k} is the wave vector inside the first BZ, and $u_{\mathbf{k}}(\mathbf{r}) = u_{\mathbf{k}}(\mathbf{r} + \mathbf{R})$ is a periodic function of the Bravais lattice. Many quantities—such as the total energy, electronic density and the total density of states—can be computed by integrating functions of \mathbf{k} over the Brillouin zone,

$$\langle A \rangle = \frac{V_{PUC}}{(2\pi)^3} \int_{BZ} A(\mathbf{k}) d\mathbf{k} \quad (2.90)$$

Attempting to compute this integral over the entire BZ would require an infinite number of \mathbf{k} points, which is intractable in practice. Instead, we can discretise the BZ into a finite number of \mathbf{k} points. In VASP, it is achieved by following the Monkhorst-Pack³⁷ scheme,

$$\mathbf{k} = \sum_{i=3}^3 \frac{n_i + s_i + \frac{1-N_i}{2}}{N_1} \mathbf{b}_i \quad (2.91)$$

where n_i are indices representing the subdivisions along each reciprocal lattice vector, s_i is an optional shift in terms of subdivisions, and N_i is the total number of subdivisions along the \mathbf{b}_i direction.

Ultimately, the Monkhorst-Pack scheme allows us to generate a uniform and symmetrical grid of \mathbf{k} points in the BZ, and, consequently, to compute integrals over the BZ by summing

over a finite number of \mathbf{k} points.

- **Plane-Wave Expansion and Cut-off Energy**

Following from our previous discussion—where we expressed the single-electron wavefunction as a combination of a periodic function and a plane wave—we can expand $u_{\mathbf{k}}(\mathbf{r})$ in terms of a set of plane waves

$$u_{\mathbf{k}}(\mathbf{r}) = \sum_{\mathbf{G}} C_{\mathbf{G}} e^{i\mathbf{G}\cdot\mathbf{r}} \quad (2.92)$$

Combining Equations 2.89 and 2.92, gives

$$\psi_{\mathbf{k}}(\mathbf{r}) = \sum_{\mathbf{G}} C_{\mathbf{k}+\mathbf{G}} e^{i(\mathbf{k}+\mathbf{G})\cdot\mathbf{r}} \quad (2.93)$$

where $C_{\mathbf{k}+\mathbf{G}}$ are the corresponding Fourier coefficients associated to the plane wave of wavevector $\mathbf{k} + \mathbf{G}$.

Noticeably, Equation 2.93 introduces a new complexity in the calculations—the evaluation of a single \mathbf{k} -point requires the summation over an infinite number of possible \mathbf{G} vectors. However, the interpretation of Equation 2.93 as solutions to the Schrödinger equation allows for the kinetic energy to be expressed as

$$E_{\text{kin}} = \frac{1}{2} |\mathbf{k} + \mathbf{G}|^2 \quad (2.94)$$

In practice, lower energy solutions are more physically relevant, thereby allowing us to truncate the infinite summation by including only plane waves whose kinetic energy does not exceed a certain cut-off energy E_{cut}

$$\frac{1}{2} |\mathbf{k} + \mathbf{G}|^2 \leq E_{\text{cut}} \quad (2.95)$$

This gives a finite expansion

$$\psi_{\mathbf{k}}(\mathbf{r}) = \sum_{|\mathbf{k}+\mathbf{G}|^2/2 \leq E_{\text{cut}}} C_{\mathbf{k}+\mathbf{G}} e^{i(\mathbf{k}+\mathbf{G})\cdot\mathbf{r}} \quad (2.96)$$

Finally, in VASP, we often set the cut-off energy based on a convergence criterion of the total energy of the system

$$\Delta E_{\text{tot}} < 1 \text{meV/atom} \quad (2.97)$$

ensuring a good description of the electronic structure of the system and keeping the calculations computationally feasible.

2.6.2.2 Projector Augmented-Wave (PAW) Method

Having explored the base concepts of the Projector Augmented-Wave (PAW) method—regarding its implementation in VASP—we can transition to the PAW formalism itself. The PAW method was first introduced by P. E. Blöchl³⁸ as a generalisation of the pseudopotential method and linear augmented plane-wave method. Later on, it was further refined by G. Kresse and J. Joubert³⁹ providing a formal relationship between ultra-soft pseudopotentials and the PAW method.

The PAW method addresses the problem of describing the valence states with high accuracy while accounting for the large variations in the all-electron (AE) wavefunction near the atomic core. It does so by introducing a transformation that maps pseudo (PS) wavefunctions—smooth and computationally efficient—onto their corresponding AE counterparts. Thereby, any AE Kohn-Sham wavefunction Ψ_n can be recovered from a PS wavefunction $\tilde{\Psi}_n$ by means of a linear transformation

$$|\Psi_n\rangle = |\tilde{\Psi}_n\rangle + \sum_i \left(|\phi_i\rangle - |\tilde{\phi}_i\rangle \right) \langle \tilde{p}_i | \tilde{\Psi}_n \rangle \quad (2.98)$$

where important elements are to be highlighted:

- AE partial wavefunctions $|\phi_i\rangle$, obtained from a reference atom.
- PS partial wavefunctions $|\tilde{\phi}_i\rangle$, which match the AE wavefunctions outside a core radius r_c .
- Projector functions $|\tilde{p}_i\rangle$, which quantify the contribution of the difference $|\phi_i\rangle - |\tilde{\phi}_i\rangle$ to be added to the PS wavefunction in order to recover the AE wavefunction. They fulfil the biorthonormality condition $\langle \tilde{p}_i | \tilde{\phi}_j \rangle = \delta_{ij}$ within the augmentation region, ultimately leading to the completeness relation $\sum_i |\tilde{\phi}_i\rangle \langle \tilde{p}_i | = \mathbb{1}$.

Additionally, in the PAW method, the total AE electronic density is expressed as

$$n(\mathbf{r}) = \tilde{n}(\mathbf{r}) + n^1(\mathbf{r}) - \tilde{n}^1(\mathbf{r}) \quad (2.99)$$

where \tilde{n} is the PS valence electronic density, n^1 is the AE one-center electronic density accounting for the contribution of the valence states inside the augmentation region, and \tilde{n}^1 is the corresponding PS one-center electronic density.

Finally, the PAW method helps us to recover the true AE electronic density by correcting the PS electronic density within the augmentation region. As a result, many electronic structure properties—such as the total energy, forces and stresses—can be accurately evaluated.

2.6.3 Equation of State (EOS)

In order to study the mechanical properties of bulk materials, it is important to establish a relationship between observables—such as the ground state total energy—and macroscopic variables like volume or pressure. In this context, the third-order Birch-Murnaghan equation of state^{40,41} provides a means to relate the total energy to the change in volume in the system. By fitting energy-volume data to this equation, one can obtain important elastic properties, including equilibrium volume and energy, the bulk modulus and its pressure derivative. This equation is given by

$$E(V) = E_0 + \frac{9}{16} V_0 B_0 \left\{ \left[\left(\frac{V_0}{V} \right)^{2/3} - 1 \right]^3 B'_0 + \left[\left(\frac{V_0}{V} \right)^{2/3} - 1 \right]^2 \left[6 - 4 \left(\frac{V_0}{V} \right)^{2/3} \right] \right\} \quad (2.100)$$

where E_0 , V_0 , B_0 and B'_0 are the equilibrium energy, volume, bulk modulus and its pressure derivative, respectively.

Equation 2.100 is utilised in this work to report the aforementioned thermodynamic properties, which are essential for understanding the material's mechanical response under compression or expansion.

2.6.4 Machine Learning Force Fields (MLFFs)

In an earlier discussion, we introduced the concept of *ab initio* molecular dynamics (AIMD) and highlighted its importance for determining the dynamical properties of a material. Nonetheless—even though VASP is highly optimised for these calculations—AIMD methods remain computationally expensive, restricting its applicability to small simulation cells and short simulation times.

In this regard, machine learning force fields (MLFFs) represent a promising alternative. These models are trained on accurate *ab initio* datasets, allowing them to learn the underlying potential energy, thereby producing fast and accurate predictions of atomic energies, forces and stresses. MLFFs can drastically reduce computational cost while minimising any human intervention and expertise required for the force field construction.

In VASP, MLFFs are implemented following an on-the-fly machine learning algorithm⁴² (see Figure 2.2). To construct the machine-learning force field several structure datasets are required. A structure dataset must define the Bravais lattice, atomic positions, total energy, forces and the stress tensor computed from first principles (FP). Given the datasets, local configurations around an atom are identified and mapped onto a set of descriptors⁴³, describing the local environment around each atom in terms of an atomic distribution function.

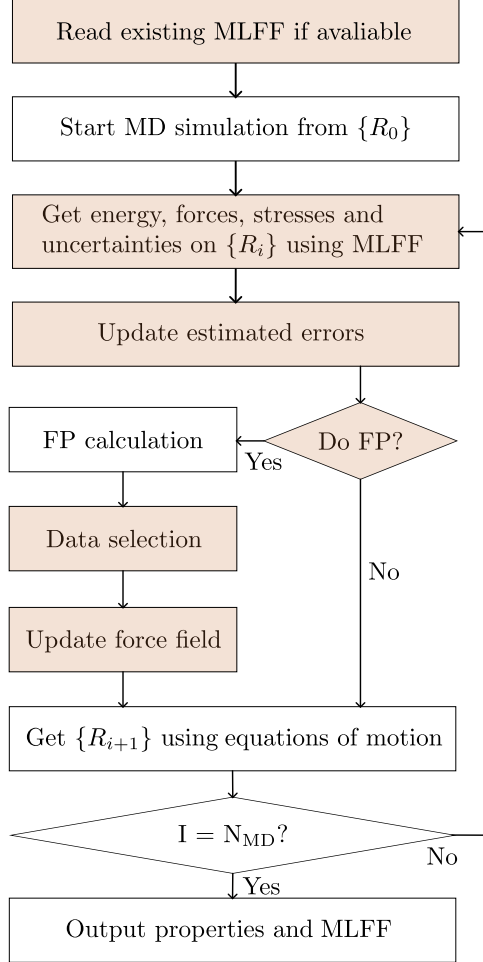


Figure 2.2: On-the-fly force field generation pipeline in VASP⁴². First, the algorithm reads the existing MLFF if available; otherwise it generates a new one. If accurate enough, a new structure is generated using the force field; otherwise, a first principles calculation is performed. If the predicted uncertainty is too large, the new structure is added to the dataset, and the force field is retrained. This oscillating process between training and prediction continues until we reach the total number of ionic steps specified in the setup.

$$\rho_i^{(2)}(r) = \frac{1}{4\pi} \int \rho(r\hat{\mathbf{r}}) d\hat{\mathbf{r}} \quad (2.101)$$

$$\rho_i^{(3)}(r, s, \theta) = \iint d\hat{\mathbf{r}} d\hat{\mathbf{s}} \delta(\hat{\mathbf{r}} \cdot \hat{\mathbf{s}} - \cos \theta) \sum_{j=1}^{N_a} \sum_{k \neq i, j} \tilde{\rho}_{ij}(r\hat{\mathbf{r}}) \tilde{\rho}_{ik}(s\hat{\mathbf{s}}) \quad (2.102)$$

Equation 2.101 defines the two-body descriptor as the probability of finding an atom $j(j \neq i)$ at a distance r from atom i . Conversely, Equation 2.102 is known as the three-body descriptor and describes the probability to find an atom $j(j \neq i)$ at a distance r from atom i and another atom $k(k \neq i, j)$ at a distance s from atom i spanning an angle $\angle kij$ between them. These descriptors are then used to construct the local potential energy functionals $U_i = F[\rho_i^{(2)}, \rho_i^{(3)}]$ upon which the force field is constructed.

The force field is then generated during AIMD simulations following the steps below:

1. The machine predicts the energy, forces, stress tensor and uncertainty for the current atomic configuration using the available force field.
2. The algorithm decided whether to perform an FP calculation or not. This decision is based on the uncertainty of the prediction. If the uncertainty is larger than a predefined threshold, the machine continues to step 3; otherwise, it proceeds to step 5.
3. The FP calculation is performed for the current structure, and the obtained dataset is then stored as a candidate for the training dataset.
4. If the number of candidate structures reaches a certain threshold, or if the uncertainty becomes too large, the algorithm updates the training set and generates a new force field.
5. Update the atomic positons and velocities. If the force field is not accurate enough, the FP energy, forces and stress tensor are used. Otherwise, those predicted by the force field are used. Afterwards, the algorithm returns to step 1 until the total number of ionic steps is reached.

Ultimately, MLFFs provide a powerful and efficient method for performing MD simulations. It combines the accuracy of AIMD with the speed of classical MD, allowing for large and complex condensed matter systems to be studied with remarkable accuracy and efficiency.

2.7 Density Functional Tight Binding (DFTB+)

Chapter 3

Methodology

This chapter outlines the methodology followed in this work to perform the computational simulations of calcium silicate hydrates (C-S-H). All the calculateions were carried out using Density Functional Tight Binding (DFTB+)—primarily in the initial stages—and subsequently with the Vienna Ab-initio Simulation Package (VASP).

We begin by describing the initial C-S-H structure, followed by a preliminary relaxation using DFTB+. Thereafter, we present the workflow adopted in VASP, detailing the main input and output files necessary for the simulations. Finally, we discuss the generation of the machine learning force field (MLFF), covering the training, refinement and testing phases.

3.1 Initial CSH Structure

The investigations performed in this work are based in the C-S-H structure proposed by Pellenq *et al.*⁴⁴. This molecular model was constructed

3.2 VASP Workflow

3.3 VASP Input & Output Files

One more section

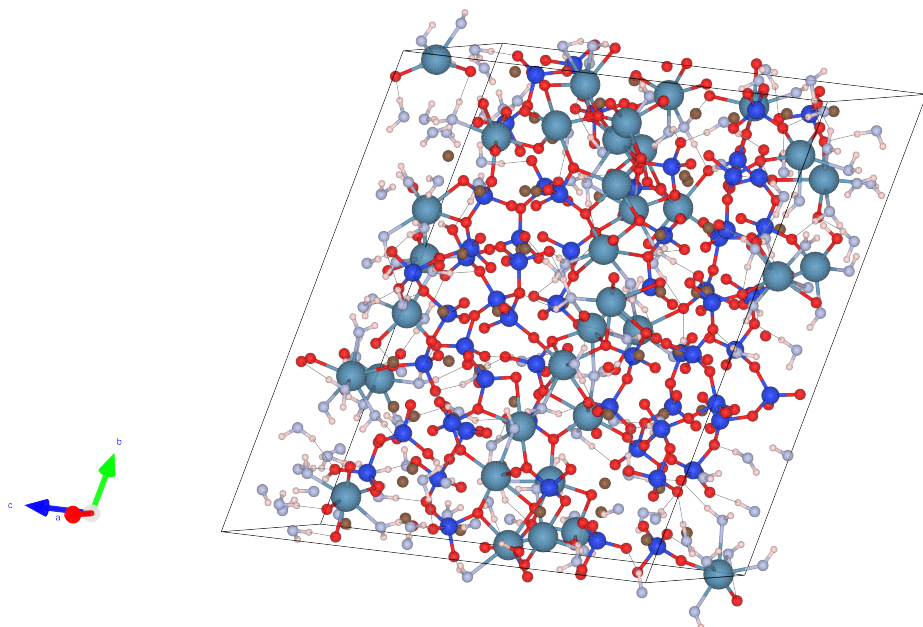


Figure 3.1: Molecular model of C-S-H proposed by Ref.⁴⁴. Lavender and white spheres are oxygen and hydrogen from water molecules respectively; light blue and brown spheres are inter and intra-layer calcium ions, respectively; electric blue and red spheres are silicon and oxygen atoms from silica tetrahedra, respectively.

3.3.1 Input Files

3.3.2 Output Files

3.4 Strucure Optimisation and Relaxation

3.4.1 Initial Relaxation with DFTB+

3.4.2 Full Structure Relaxation with VASP

3.5 Machine Learning Force Field Generation

3.5.1 MLFF Training

3.5.2 MLFF Refinement

3.5.3 MLFF Testing

One last section

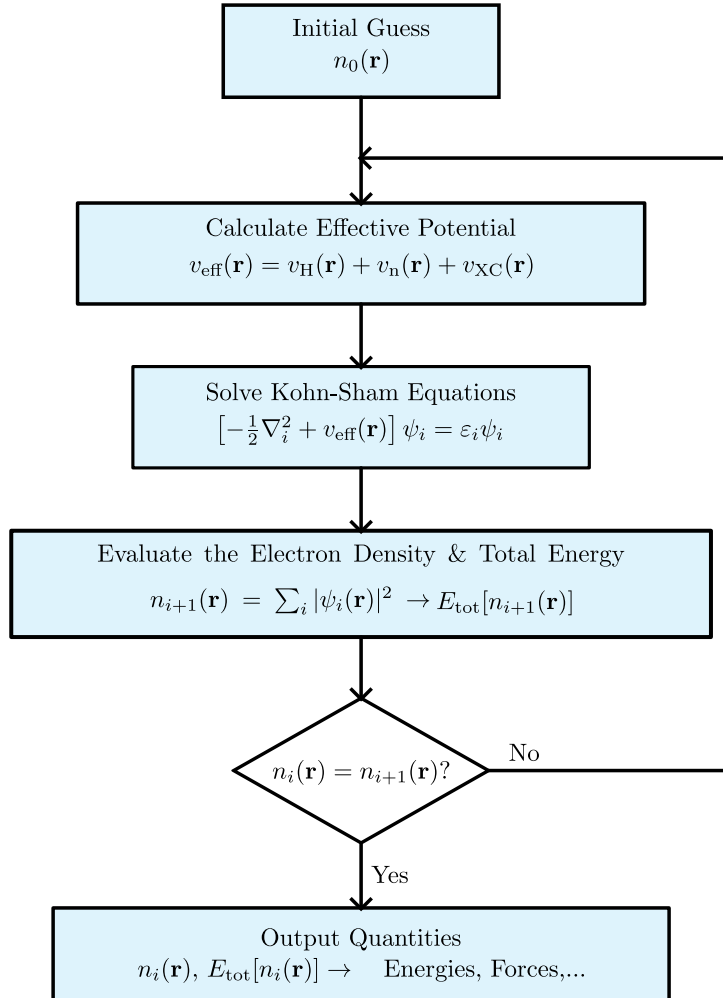


Figure 3.2: Self-consistent field (SFC) cycle in VASP for DFT calculations adapted from Ref.¹¹. The entire cycle starts with an initial guess of the electronic density $n_0(\mathbf{r})$, which then is used to calculate the effective potential $v_{\text{eff}}(\mathbf{r})$. Then, the resulting potential is used to solve the Kohn-Sham equations, from which single-electron wavefunctions $\psi_i(\mathbf{r})$ are obtained. Consequently, the new electronic density $n_{i+1}(\mathbf{r})$ is calculated. Should the old and new densities be close enough—up to a predefined threshold—the cycle stops, and the final electronic density is used to calculate the energies, forces and stress tensor of the system. Otherwise, the cycle repeats itself until convergence is achieved.

Ca Si O H			
1.0			
13.18335946	0.18445997	0.00755401	
-16.45244030	24.21622147	-0.00875423	
1.20664987	-0.82375620	23.18729854	
Ca Si O H			
99	60	323	208
Direct			
0.38821570	0.10613519	0.29312228	
0.37259751	0.56538816	0.26881558	
0.37469040	0.31600944	0.23882914	
0.35542617	0.78384113	0.38748504	
0.91347068	0.11233954	0.31634176	
0.90355777	0.57838562	0.23567872	
0.87836092	0.32109531	0.25338100	
0.84529168	0.81264469	0.29236748	
0.11769176	0.02588977	0.65372010	

Figure 3.3: Unit cell structure in fractional coordinates for the C–S–H (Calcium-Silicate-Hydrate) system. The lattice vectors, atomic species (99 Ca, 60 Si, 323 O, 208 H), and the first 9 atomic positions are shown. All coordinates are expressed in direct (fractional) form.

Chapter 4

Results & Discussion

4.1 Convergency Tests

4.1.1 Cut-off Energy

4.1.2 K-Points Sampling

4.2 Density of States (DOS)

Hello

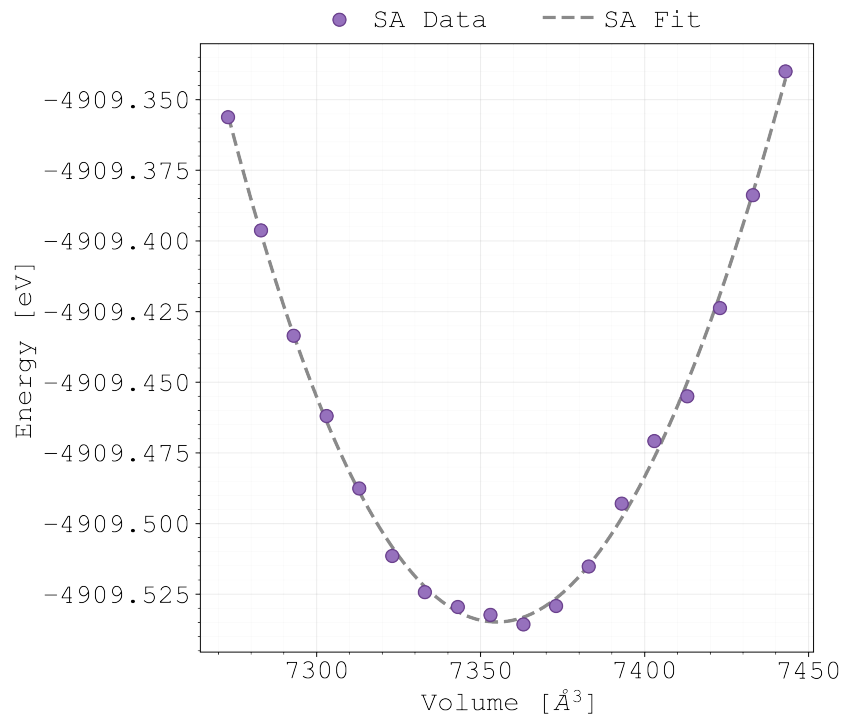


Figure 4.1: A schematic representation of the DFT formalism. The many-body wavefunction is replaced by a single-particle wavefunction, which is used to calculate the electron density. The electron density is then used to calculate the total energy of the system. Adapted from¹⁰.

Bibliography

- [1] Paulo J. M. Monteiro, Sabbie A. Miller, and Arpad Horvath. “Towards Sustainable Concrete”. In: *Nature Materials* 16.7 (July 2017), pp. 698–699. ISSN: 1476-4660. DOI: 10.1038/nmat4930. (Visited on 03/16/2025).
- [2] Henri Van Damme. “Concrete Material Science: Past, Present, and Future Innovations”. In: *Cement and Concrete Research*. SI : Digital Concrete 2018 112 (Oct. 2018), pp. 5–24. ISSN: 0008-8846. DOI: 10.1016/j.cemconres.2018.05.002. (Visited on 03/16/2025).
- [3] P. Kumar Mehta and Paulo J. M. Monteiro. “Introduction”. In: *Concrete: Microstructure, Properties, and Materials*. 4th Edition. New York: McGraw-Hill Education, 2014. ISBN: 978-0-07-179787-0. URL: <https://www.accessengineeringlibrary.com/content/book/9780071797870/chapter/chapter1>.
- [4] Styliani Papatzani, Kevin Paine, and Juliana Calabria-Holley. “A Comprehensive Review of the Models on the Nanostructure of Calcium Silicate Hydrates”. In: *Construction and Building Materials* 74 (Jan. 2015), pp. 219–234. ISSN: 0950-0618. DOI: 10.1016/j.conbuildmat.2014.10.029. (Visited on 03/16/2025).
- [5] Katerina Ioannidou et al. “Mesoscale Texture of Cement Hydrates”. In: *Proceedings of the National Academy of Sciences* 113.8 (Feb. 2016), pp. 2029–2034. DOI: 10.1073/pnas.1520487113. (Visited on 01/16/2025).
- [6] Mohammad Javad Abdolhosseini Qomi, Mathieu Bauchy, and Roland J.-M. Pellenq. “Nanoscale Composition-Texture-Property Relation in Calcium-Silicate-Hydrates”. In: *Handbook of Materials Modeling: Applications: Current and Emerging Materials*. Ed. by Wanda Andreoni and Sidney Yip. Cham: Springer International Publishing, 2020, pp. 1761–1792. ISBN: 978-3-319-44680-6. DOI: 10.1007/978-3-319-44680-6_128. (Visited on 09/24/2024).
- [7] Ashraf A. Bahraq et al. “Molecular Simulation of Cement-Based Materials and Their Properties”. In: *Engineering* 15 (Aug. 2022), pp. 165–178. ISSN: 2095-8099. DOI: 10.1016/j.eng.2021.06.023. (Visited on 09/17/2024).

- [8] Emmy M. Foley, Jung J. Kim, and M. M. Reda Taha. "Synthesis and Nano-Mechanical Characterization of Calcium-Silicate-Hydrate (C-S-H) Made with 1.5 CaO/SiO₂ Mixture". In: *Cement and Concrete Research* 42.9 (Sept. 2012), pp. 1225–1232. ISSN: 0008-8846. DOI: 10.1016/j.cemconres.2012.05.014. (Visited on 06/05/2025).
- [9] Mohammad Javad Abdolhosseini Qomi, Franz-Josef Ulm, and Roland J.-M. Pellenq. "Physical Origins of Thermal Properties of Cement Paste". In: *Physical Review Applied* 3.6 (June 2015), p. 064010. DOI: 10.1103/PhysRevApplied.3.064010. (Visited on 09/11/2024).
- [10] F. Giustino. *Materials Modelling Using Density Functional Theory: Properties and Predictions*. Oxford University Press, 2014. ISBN: 978-0-19-966244-9. URL: <https://books.google.com.ec/books?id=Fz0TAwAAQBAJ>.
- [11] D.S. Sholl and J.A. Steckel. *Density Functional Theory: A Practical Introduction*. Wiley, 2023. ISBN: 978-1-119-84086-2. URL: <https://books.google.com.ec/books?id=BR-gEAAAQBAJ>.
- [12] E. Kaxiras. *Atomic and Electronic Structure of Solids*. Cambridge University Press, 2003. ISBN: 978-0-521-81010-4. URL: https://books.google.com.ec/books?id=WTL_vgbWpHEC.
- [13] R.M. Martin, L. Reining, and D.M. Ceperley. *Interacting Electrons*. Cambridge University Press, 2016. ISBN: 978-0-521-87150-1. URL: <https://books.google.com.ec/books?id=ch1CDAAAQBAJ>.
- [14] T. Helgaker, P. Jorgensen, and J. Olsen. *Molecular Electronic-Structure Theory*. Wiley, 2014. ISBN: 978-1-119-01955-8. URL: <https://books.google.com.ec/books?id=lnVLBAAAQBAJ>.
- [15] D. Feng and G. Jin. *Introduction to Condensed Matter Physics, Volume 1*. World Scientific Publishing Company, 2005. ISBN: 978-981-310-219-4. URL: <https://books.google.com.ec/books?id=IM47DQAAQBAJ>.
- [16] D. R. Hartree. "The Wave Mechanics of an Atom with a Non-Coulomb Central Field. Part I. Theory and Methods". In: *Mathematical Proceedings of the Cambridge Philosophical Society* 24.1 (Jan. 1928), pp. 89–110. ISSN: 1469-8064, 0305-0041. DOI: 10.1017/S0305004100011919. (Visited on 07/10/2025).
- [17] V. Fock. "Näherungsmethode zur Lösung des quantenmechanischen Mehrkörperproblems". In: *Zeitschrift für Physik* 61.1 (Jan. 1930), pp. 126–148. ISSN: 0044-3328. DOI: 10.1007/BF01340294. (Visited on 07/10/2025).
- [18] R.M. Martin. *Electronic Structure: Basic Theory and Practical Methods*. Cambridge University Press, 2020. ISBN: 978-1-108-42990-0. URL: <https://books.google.com.ec/books?id=wvXvDwAAQBAJ>.
- [19] P. Hohenberg and W. Kohn. "Inhomogeneous Electron Gas". In: *Physical Review* 136.3B (Nov. 1964), B864–B871. DOI: 10.1103/PhysRev.136.B864. (Visited on 07/12/2025).

- [20] W. Kohn and L. J. Sham. “Self-Consistent Equations Including Exchange and Correlation Effects”. In: *Physical Review* 140.4A (Nov. 1965), A1133–A1138. DOI: [10.1103/PhysRev.140.A1133](https://doi.org/10.1103/PhysRev.140.A1133). (Visited on 07/12/2025).
- [21] W. Kohn. “Nobel Lecture: Electronic Structure of Matter—Wave Functions and Density Functionals”. In: *Reviews of Modern Physics* 71.5 (1999), pp. 1253–1266. DOI: [10.1103/RevModPhys.71.1253](https://doi.org/10.1103/RevModPhys.71.1253).
- [22] D. M. Ceperley and B. J. Alder. “Ground State of the Electron Gas by a Stochastic Method”. In: *Physical Review Letters* 45.7 (Aug. 1980), pp. 566–569. DOI: [10.1103/PhysRevLett.45.566](https://doi.org/10.1103/PhysRevLett.45.566). (Visited on 07/19/2025).
- [23] J. P. Perdew and Alex Zunger. “Self-Interaction Correction to Density-Functional Approximations for Many-Electron Systems”. In: *Physical Review B* 23.10 (May 1981), pp. 5048–5079. DOI: [10.1103/PhysRevB.23.5048](https://doi.org/10.1103/PhysRevB.23.5048). (Visited on 07/19/2025).
- [24] John P. Perdew, Kieron Burke, and Matthias Ernzerhof. “Generalized Gradient Approximation Made Simple”. In: *Physical Review Letters* 77.18 (Oct. 1996), pp. 3865–3868. DOI: [10.1103/PhysRevLett.77.3865](https://doi.org/10.1103/PhysRevLett.77.3865). (Visited on 07/19/2025).
- [25] John P. Perdew et al. “Restoring the Density-Gradient Expansion for Exchange in Solids and Surfaces”. In: *Physical Review Letters* 100.13 (Apr. 2008), p. 136406. DOI: [10.1103/PhysRevLett.100.136406](https://doi.org/10.1103/PhysRevLett.100.136406). (Visited on 07/21/2025).
- [26] Jochen Heyd, Gustavo E. Scuseria, and Matthias Ernzerhof. “Hybrid Functionals Based on a Screened Coulomb Potential”. In: *The Journal of Chemical Physics* 118.18 (May 2003), pp. 8207–8215. ISSN: 0021-9606. DOI: [10.1063/1.1564060](https://doi.org/10.1063/1.1564060). (Visited on 07/19/2025).
- [27] Jonathan E. Moussa, Peter A. Schultz, and James R. Chelikowsky. “Analysis of the Heyd-Scuseria-Ernzerhof Density Functional Parameter Space”. In: *The Journal of Chemical Physics* 136.20 (May 2012). ISSN: 0021-9606, 1089-7690. DOI: [10.1063/1.4722993](https://doi.org/10.1063/1.4722993). arXiv: [1205.4999 \[cond-mat\]](https://arxiv.org/abs/1205.4999). (Visited on 07/22/2025).
- [28] John P. Perdew and Karla Schmidt. “Jacob’s Ladder of Density Functional Approximations for the Exchange-Correlation Energy”. In: *AIP Conference Proceedings* 577.1 (July 2001), pp. 1–20. ISSN: 0094-243X. DOI: [10.1063/1.1390175](https://doi.org/10.1063/1.1390175). (Visited on 07/19/2025).
- [29] D. Marx and J. Hutter. *Ab Initio Molecular Dynamics: Basic Theory and Advanced Methods*. Cambridge University Press, 2009. ISBN: 978-1-139-47719-2. URL: <https://books.google.com.ec/books?id=VRZUw8Wk4CIC>.
- [30] Thomas D. Kühne. “Ab-Initio Molecular Dynamics”. In: *WIREs Computational Molecular Science* 4.4 (July 2014), pp. 391–406. ISSN: 1759-0876, 1759-0884. DOI: [10.1002/wcms.1176](https://doi.org/10.1002/wcms.1176). arXiv: [1201.5945 \[physics\]](https://arxiv.org/abs/1201.5945). (Visited on 07/26/2025).
- [31] R. P. Feynman. “Forces in Molecules”. In: *Physical Review* 56.4 (1939), pp. 340–343. DOI: [10.1103/PhysRev.56.340](https://doi.org/10.1103/PhysRev.56.340).

- [32] Peter Politzer and Jane S. Murray. “The Hellmann-Feynman Theorem: A Perspective”. In: *Journal of Molecular Modeling* 24.9 (Aug. 2018), p. 266. ISSN: 0948-5023. DOI: 10.1007/s00894-018-3784-7. (Visited on 07/28/2025).
- [33] M.E. Tuckerman. *Statistical Mechanics: Theory and Molecular Simulation*. Oxford Graduate Texts. Oxford University Press, 2023. ISBN: 978-0-19-882556-2. URL: <https://books.google.com.ec/books?id=EEPJEAAAQBAJ>.
- [34] D. Frenkel and B. Smit. *Understanding Molecular Simulation: From Algorithms to Applications*. Academic Press, 2023. ISBN: 978-0-323-91318-8. URL: <https://books.google.com.ec/books?id=jyipEAAAQBAJ>.
- [35] Jürgen Hafner. “Ab-Initio Simulations of Materials Using VASP: Density-functional Theory and Beyond”. In: *Journal of Computational Chemistry* 29.13 (2008), pp. 2044–2078. DOI: 10.1002/jcc.21057. eprint: <https://onlinelibrary.wiley.com/doi/pdf/10.1002/jcc.21057>.
- [36] H. Hellmann. “A New Approximation Method in the Problem of Many Electrons”. In: *The Journal of Chemical Physics* 3.1 (Jan. 1935), p. 61. ISSN: 0021-9606. DOI: 10.1063/1.1749559. (Visited on 07/30/2025).
- [37] Hendrik J. Monkhorst and James D. Pack. “Special Points for Brillouin-zone Integrations”. In: *Physical Review B* 13.12 (June 1976), pp. 5188–5192. DOI: 10.1103/PhysRevB.13.5188. (Visited on 08/01/2025).
- [38] P. E. Blöchl. “Projector Augmented-Wave Method”. In: *Physical Review B* 50.24 (Dec. 1994), pp. 17953–17979. DOI: 10.1103/PhysRevB.50.17953. (Visited on 07/30/2025).
- [39] G. Kresse and D. Joubert. “From Ultrasoft Pseudopotentials to the Projector Augmented-Wave Method”. In: *Physical Review B* 59.3 (Jan. 1999), pp. 1758–1775. DOI: 10.1103/PhysRevB.59.1758. (Visited on 07/30/2025).
- [40] Francis Birch. “Finite Elastic Strain of Cubic Crystals”. In: *Physical Review* 71.11 (June 1947), pp. 809–824. DOI: 10.1103/PhysRev.71.809. (Visited on 07/30/2025).
- [41] J.P. Poirier. *Introduction to the Physics of the Earth’s Interior*. Introduction to the Physics of the Earth’s Interior. Cambridge University Press, 2000. ISBN: 978-0-521-66392-2. URL: https://books.google.com.ec/books?id=_Y0C186XPHoC.
- [42] Ryosuke Jinnouchi, Ferenc Karsai, and Georg Kresse. “On-the-Fly Machine Learning Force Field Generation: Application to Melting Points”. In: *Physical Review B* 100.1 (July 2019), p. 014105. DOI: 10.1103/PhysRevB.100.014105. (Visited on 07/31/2025).
- [43] Ryosuke Jinnouchi et al. “Descriptors Representing Two- and Three-Body Atomic Distributions and Their Effects on the Accuracy of Machine-Learned Inter-Atomic Potentials”. In: *The Journal of Chemical Physics* 152.23 (June 2020). ISSN: 0021-9606. DOI: 10.1063/5.0009491. (Visited on 07/31/2025).

- [44] Roland J.-M. Pellenq et al. “A Realistic Molecular Model of Cement Hydrates”. In: *Proceedings of the National Academy of Sciences* 106.38 (Sept. 2009), pp. 16102–16107. DOI: [10.1073/pnas.0902180106](https://doi.org/10.1073/pnas.0902180106). (Visited on 09/11/2024).